ACS Sustainable Chemistry & Engineering

pubs.acs.org/ascecg

Research Article

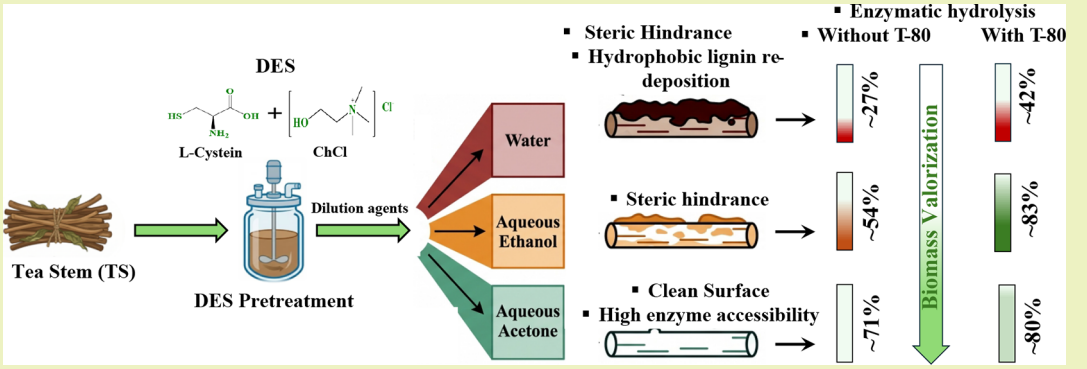
Beyond Pretreatment Severity: Recovery-Stage Antisolvent Selection Controls Biomass Recalcitrance, Enzymatic Accessibility, and Lignin Quality in Deep Eutectic Solvent Fractionation

Usama Shakeel, Ying Zeng, Furong Zheng, Jiaqi Guo, Wenyuan Zhu, Mohamed El-Sakhawy, Carolina Krebs de Souza, and Junlong Song*

Cite This: https://doi.org/10.1021/acssuschemeng.6c11956

Read Online

ACCESS | Metrics & More | Article Recommendations | Supporting Information



ABSTRACT: Deep eutectic solvent (DES) pretreatment disrupts the lignocellulosic biomass (LCB) matrix, yet efficacy is largely attributed to upstream chemical severity, while post-pretreatment antisolvent dilution and phase separation is treated as a passive downstream operation. This study investigated the fractionation of tea-stems using a ChCl:L-Cys DES, revealing that downstream phase separation induced by antisolvent dilution critically dictates LCB valorization. Diluting identically DES-pretreated media with 50% aqueous acetone, 50% aqueous ethanol, or water yielded enzymatic hydrolysis (EH) of 71.1%, 54.3%, and 26.8%, demonstrating an influence of antisolvent selection on post-pretreatment fractionation and substrate accessibility. Aqueous acetone retained more solubilized components, whereas polar media promoted lignin redistribution and redeposition. Redeposited lignin sterically shielded cellulose and promoted irreversible enzyme adsorption, indicating that hydrophobic interactions can outweigh electrostatic repulsion. Antisolvent selection thus emerges as a recovery-stage variable governing substrate recalcitrance and lignin quality, proving essential for optimizing biorefineries and converting unutilized biomass into valuable coproducts.

KEYWORDS: *biomass valorization, DES pretreatment, antisolvent phase separation, biomass recalcitrance, quartz crystal microbalance (QCM)*

1. INTRODUCTION

The transition from fossil resources to lignocellulosic biomass (LCB)-based biorefining demands an effective pretreatment step capable of disrupting the recalcitrant LCB matrix while preserving the value of the resulting carbohydrate and lignin fractions.[1] Among various pretreatment strategies, deep eutectic solvent (DES) pretreatment has emerged as a sustainable approach because of its economic viability, low toxicity, renewability, and tunable physicochemical properties.[2] Driven by its unique polarity and hydrogen-bonding (H-bonding) capacity, choline chloride (ChCl)-based acidic DESs can disrupt the LCB matrix through cleavage of lignin-carbohydrate complexes (LCCs).[3] However, the acidic environment also generates reactive benzyl carbocations that are susceptible to C−C coupling, resulting in condensed lignin structures that compromise downstream valorization.[1,4] Sulfur nucleophiles, particularly L-cysteine monohydrochloride (L-Cys), have therefore emerged as promising stabilizing agents. Mechanistically, the soft nucleophilic thiol (-SH) moiety of L-Cys exhibits a pronounced affinity for benzylic carbocations, trapping these reactive intermediates and thereby preserving native β-O-4 linkages.[5] Despite the

Received: October 14, 2026
Revised: November 10, 2026
Accepted: November 13, 2026

ACS Publications © XXXX American Chemical Society

advantages of this trapping pathway, direct integration of reactive nucleophiles such as L-Cys into structurally tunable amino acid-based deep eutectic solvents (AA-DESs) remains limited,[6−8] reflecting the challenge of balancing the acidity required for efficient biomass deconstruction with the chemical stability of the nucleophilic thiol group.[9,10]

While strategically designed L-Cys-based DESs can suppress lignin condensation during pretreatment, a subsequent dilution step remains necessary for solid−liquid separation and DES recovery. Among available recovery approaches, antisolvent addition is widely applied because it is rapid, straightforward, and scalable.[11,12] However, the physicochemical properties of water, ethanol, and acetone can alter the solvation of dissolved lignin, carbohydrates, and LCC-derived fragments during DES dilution. Although a few DES studies have reported effects of antisolvent selection on delignification or enzymatic hydrolysis (EH), its role has seldom been investigated independently of pretreatment severity. Consequently, how recovery-stage antisolvent selection influences substrate recalcitrance, lignin recovery, and enzymatic accessibility remains unresolved.[7,13] This gap is particularly important, as substrates identically pretreated under the same pretreatment severity may develop markedly different compositions and surface characteristics depending on the solvent environment during DES recovery. Changes in the solvent environment during DES dilution may alter the solubility and phase behavior of dissolved lignin and associated biomass-derived components, promoting their selective precipitation and redistribution onto the pretreated residue. Such recovery-stage redistribution may subsequently affect cellulose accessibility and enzyme−substrate interactions.

Accordingly, this study decouples upstream chemical deconstruction from downstream phase separation under identical DES pretreatment while varying only the antisolvent. Water, 50% aqueous ethanol, and 50% aqueous acetone were compared to assess how recovery-stage antisolvent selection governs lignin recovery, residue composition/morphology, enzymatic accessibility, and recovered lignin structure. From an integrated biorefinery perspective, fractionation performance was evaluated by lignin and the production of a carbohydrate-rich residue amenable to EH, rather than carbohydrate retention alone. QCM-D was further employed to resolve enzyme-substrate and lignin−enzyme interactions, particularly enzyme adsorption and retention at these interfaces, and to determine whether T-80 can mitigate antisolvent-induced nonproductive binding. By isolating the recovery stage from pretreatment severity, this work establishes a structure−interface−performance relationship linking antisolvent-induced phase separation to lignin redistribution, substrate recalcitrance, and downstream biomass valorization.

2. MATERIALS AND METHODS

Waste tea stems (TS, *Camellia sinensis*) were purchased (Fujian, China), washed with water, sun-dried for 2−3 days until no visible surface moisture remained, and milled to pass through a 40 mesh. Choline chloride (ChCl), L-cysteine monohydrochloride (L-Cys), trifluoro acetic acid (TFAA), Tween-80 (T-80), deionized water (DI water), ethanol, acetone, and other chemicals used in this study were purchased from Macklin (Shanghai, China). In this study, a cellulase enzyme blend (CAS 9012-54-8) was used for cellulose hydrolysis.

2.1. DES Preparation, Pretreatment, and Dilution of DES Pretreatment Media

The DES was prepared according to our previously published protocol. Briefly, choline chloride (ChCl) and L-cysteine (L-Cys) were mixed at a 1:1 molar ratio and heated at 80 °C until a homogeneous, slightly yellowish, and viscous transparent liquid was formed.[1]

The prepared DES was employed for TS pretreatment under previously established conditions with minor modifications.[1] Briefly, TS was mixed with DES at a 1:20 solid-to-liquid ratio and heated at 130 °C for 60 min. Following pretreatment, without prior solid−liquid separation, the entire reaction mixture containing both the pretreated tea-stem residue and DES liquor was directly diluted with one of three antisolvents: 50% aqueous acetone, 50% aqueous ethanol, or DI water, at a DES-to-antisolvent ratio of 1:3. Upon addition, the reaction media were gently homogenized with a glass rod for 1−2 min before filtration to separate the pretreated residues from the liquid fraction. The residues were washed three times with their respective antisolvent, and all supernatants were collected for subsequent recovery. The pretreated residues were rinsed with DI water and freeze-dried.[1] The DI-water-rinsed and freeze-dried residues were subsequently used for enzymatic hydrolysis and physicochemical characterization.

The collected liquid fractions were concentrated under reduced pressure until a viscous DES remained. This recovered DES was diluted with five volumes of DI water, and the pH was adjusted to 1.5−2.0 to ensure efficient lignin precipitation. Finally, the precipitated lignin was recovered via centrifugation, washed with acidic water (pH 1.5−2.0), and freeze-dried.

The recovered pretreated residues are designated as R-Ac, R-EtOH, and R-W, corresponding to the respective dilution reagents: 50% aqueous acetone, 50% aqueous ethanol, and DI water. Similarly, the regenerated lignin is labeled as L-Ac, L-EtOH, and L-W. Lignin extracted from the untreated biomass (Raw-TS) is designated as L-MWL (milled wood lignin). Moreover, the lignins extracted from the pretreated residues (R-Ac, R-EtOH, and R-W) to investigate the interaction of residual lignin and enzymes (QCM-D section) were named as R-L_{Ac}, R-L_{EtOH}, and R-L_{W}.

2.2. Quartz Crystal Microbalance (QCM)

The interactions of cellulase enzymes with the un/pretreated residues and the lignin extracted from the corresponding substrates were investigated using a QCM-D E4 system (Biolin Scientific, Sweden). Briefly, un/pretreated residues were first mildly ball-milled (2 h) and then fully dissolved in an 8% LiCl/DMSO solution by stirring at room temperature for 48 h, followed by heating at 60 °C for 12 h.

Prior to coating, QCM sensors were cleaned to ensure surface purity. For cleaning, the sensors were immersed in a 5:1:1 (v/v/v) mixture of DI water, ammonium hydroxide (25% NH_4OH), and hydrogen peroxide (30% H_2O_2) at 80 °C for 15 min, followed by thorough rinsing with DI water and drying under a nitrogen stream. The dissolved lignin/residue solutions (in 8% LiCl/DMSO) were subsequently spin-coated onto the sensors (30 μL sample × 07-time coating). A uniform coating protocol was applied to all samples at 2000 rpm for 20 s with an acceleration rate of 1750 rpm s^{-1}. The resulting films served as standardized model interfaces for comparative QCM-D analysis and were not intended to reproduce the native three-dimensional morphology of the un/pretreated residues. Following coating, the sensors were dried at room temperature for 24 h, then gently rinsed with DI water to remove excess LiCl/DMSO solution, dried at 60 °C for 12 h, and stored in a vacuum desiccator until use.[14,15]

A sodium citrate buffer (pH 4.8) served as the mobile phase (injection rate of 100 μL/min, 25 °C); an enzyme solution (0.1 g/L) was used to investigate the adsorption of enzymes onto the lignin and pretreated substrate films, and a T-80 solution (0.02 mg/mL) was used as a surfactant to investigate its impact on substrate hydrolysis. After the enzymes of T-80, the same buffer was used for rinsing, and the obtained results were used to evaluate the % Ir/reversibility (eq. 7) adsorption. The adsorbed mass (ng/cm^2) was calculated from the frequency shift (Δf) using the following Sauerbrey equation eq. 1:

$$\Delta m = -C.\Delta f \quad (1)$$

https://doi.org/10.1021/acssuschemeng.6c11956
ACS Sustainable Chem. Eng. XXXX, XXX, XXX−XXX

where C is the mass sensitivity constant of sensor (C = 17.7 ng/cm^2/Hz at a fundamental resonance frequency of 5 MHz).[15]

Pseudo-first-order adsorption kinetics of the enzymes and surfactants onto the pretreated residue films and lignin were determined from the real-time Δf vs time curves, fitted using the Box-Lucas 1 function (Eq. 2) via nonlinear exponential regression, which yielded excellent fits (r^2 >0.99−0.98) consistent with the enzyme being present in excess relative to the immobilized lignin substrate throughout the reaction:

$$\Delta f(t) = \Delta f_{max} \cdot \left(1 - e^{-k_{ads}(t)}\right) \quad (2)$$

where the $\Delta f(t)$ corresponds to the frequency shift at time t, Δf_{max} attributed to the maximum frequency shift representing surface saturation, and k_{ads} represents the initial rate of adsorption.

The equation was further simplified to calculate the initial hydrolysis velocity V_0 (Hz/s).

Expanding the function:

$$\Delta f(t) = \Delta f_{max} - \Delta f_{max} e^{-k_{ads}t} \quad (3)$$

Taking the first derivative with respect to (t), considering the Δf_{max} zero, and applying the chain rule to the exponential term:

$$\frac{d(\Delta f)}{dt} = 0 - \left[\Delta f_{max} \cdot (-k_{ads}) \cdot e^{-k_{ads}t}\right] \quad (4)$$

Simplification of derivatives, the double negatives cancel out, giving the velocity at any given time t:

$$V(t) = \Delta f_{max} \cdot k_{ads} \cdot e^{-k_{ads}t} \quad (5)$$

At the exact moment of hydrolysis (t = 0), the exponential term becomes e^0, and any number to the power of zero equals 1:

$$V_0 = \Delta f_{max} \cdot k_{ads} \quad (6)$$

The initial hydrolysis velocity V_0 (Hz/s), representing the instantaneous rate of hydrolysis and mass removal at the exact onset of enzymatic cleavage (t = 0), is derived mathematically from the first derivative of the Box-Lucas 1 function.

Furthermore, high-affinity binding and weak physical entrapment within the hydrodynamic boundary layer were calculated by determining the reversibility of the initial adsorption complexes. Briefly, the irreversibility fraction (%) was calculated by comparing the frequency shift following a prolonged buffer wash to the maximum frequency shift achieved during the initial adsorption phase:

$$Irreversibility\ (\%) = \left(\frac{\Delta f_{final}}{\Delta f_{\max(adsorption)}}\right) \times 100 \quad (7)$$

Vapor-phase chemical derivatization of hydroxyl (−OH) groups in the extracted lignin from pretreated residues was performed in a glass reaction vessel, maintaining close proximity between the samples and TFAA while avoiding direct physical contact to prevent unintended sample modification. Briefly, 3 mL of TFAA was placed in the reaction vessel alongside lignin samples, which were spread as thin layers on sample holders. The vessel was sealed, and a mild vacuum was applied to facilitate TFAA evaporation over a 3 h period; this process was repeated twice to ensure maximum derivatization. Subsequently, the TFAA containing vessel was removed, and the samples were maintained under vacuum for 48 h to eliminate any nonspecifically adsorbed fluorine (F). The surface functional groups of the derivatized lignin samples were then characterized via XPS using a Thermo Scientific ESCALAB 250Xi instrument equipped with a monochromated Al Ka X-ray source (hv = 1486.6 eV), with spectral deconvolution performed using XPSPEAK 4.1 software.[16]

DES pretreatment/fractionation, compositional analysis, and enzymatic hydrolysis were independently performed in triplicate (n = 3), and the results are expressed as mean ± standard deviation (S.D.). The corresponding S.D. is presented as error bars in the relevant figures.

3. RESULTS AND DISCUSSION

3.1. Antisolvent Selection Dictates Macroscopic Fractionation and Substrate Digestibility

3.1.1. Component Analysis of Un/Pretreated Residues.

The DES pretreatment of TS was carried out according to our previous study, with slight modifications. Briefly, the pretreatment was conducted at 130 °C for 1 h with a solid-to-liquid (S/L) ratio of 1:20 and then diluted using different antisolvents, including 50% aqueous acetone, 50% aqueous ethanol, and pure water, to reduce viscosity and facilitate the separation of the liquid stream from the pretreated residues. Results revealed that despite identical pretreatment conditions, the reaction media diluted with these different solvents exhibited varying weight loss, suggesting the heterogeneous structural characteristics of pretreated residues (Figure 1A). Dilution with aqueous acetone, aqueous ethanol, and water resulted in weight losses of 47.71%, 41.34%, and 39.73%, respectively. The greater weight loss observed for R-Ac indicates a higher net removal of biomass-derived components during fractionation, although this parameter alone does not resolve their subsequent partitioning between the recovered solid and liquid fractions.

Beyond overall weight loss, the type of antisolvent significantly influenced the extracted lignin yield. Aqueous acetone enabled the highest lignin recovery (57.12%), whereas this yield dropped to 44.91% and ∼8.54% when using aqueous ethanol and water, respectively. These values represent the final lignin recovered from the liquid fraction relative to the lignin initially present in the raw biomass, revealing a pronounced antisolvent-dependent fractionation of lignin between the recovered solid and liquid fractions.[17]

Compositional analysis further revealed that the acetone-precipitated residue (R-Ac) contained 53.4% cellulose, 8.98% hemicellulose, and 9.16% lignin. In contrast, R-EtOH and R-W exhibited considerably different compositions. Specifically, R-EtOH comprised 45.98% cellulose, 12.97% hemicellulose, and 14.34% lignin, while R-W contained 41.43% cellulose, 10.97% hemicellulose, and 19.63% lignin. These results indicate that R-EtOH retained ∼44.43% more hemicellulose than R-Ac. Furthermore, R-EtOH and R-W exhibited 56.55% and 114.30% more lignin, respectively, compared to R-Ac. Despite this substantial lignin redeposition on the R-W residue, its overall weight loss of 39.73% indicates that water remained highly effective at dissolving and washing away degraded carbohydrates and other water-soluble extractives. Ultimately, while aqueous acetone, aqueous ethanol, and water all effectively lowered the DES viscosity to facilitate handling, the unintended precipitation caused by these antisolvents significantly altered both the lignin yield and the substrate composition, which will potentially impact subsequent downstream valorization.[12]

Importantly, while high-pretreatment severities are avoided to prevent lignin condensation or surface redeposition of pseudo-lignin or relocalized lignin, results reveal that incompatible antisolvents also have potential to induce similar adverse effects. The redeposition of lignin creates unproductive enzyme binding sites that reduce EH efficiency, while the concurrent

https://doi.org/10.1021/acssuschemeng.6c11956
ACS Sustainable Chem. Eng. XXXX, XXX, XXX−XXX

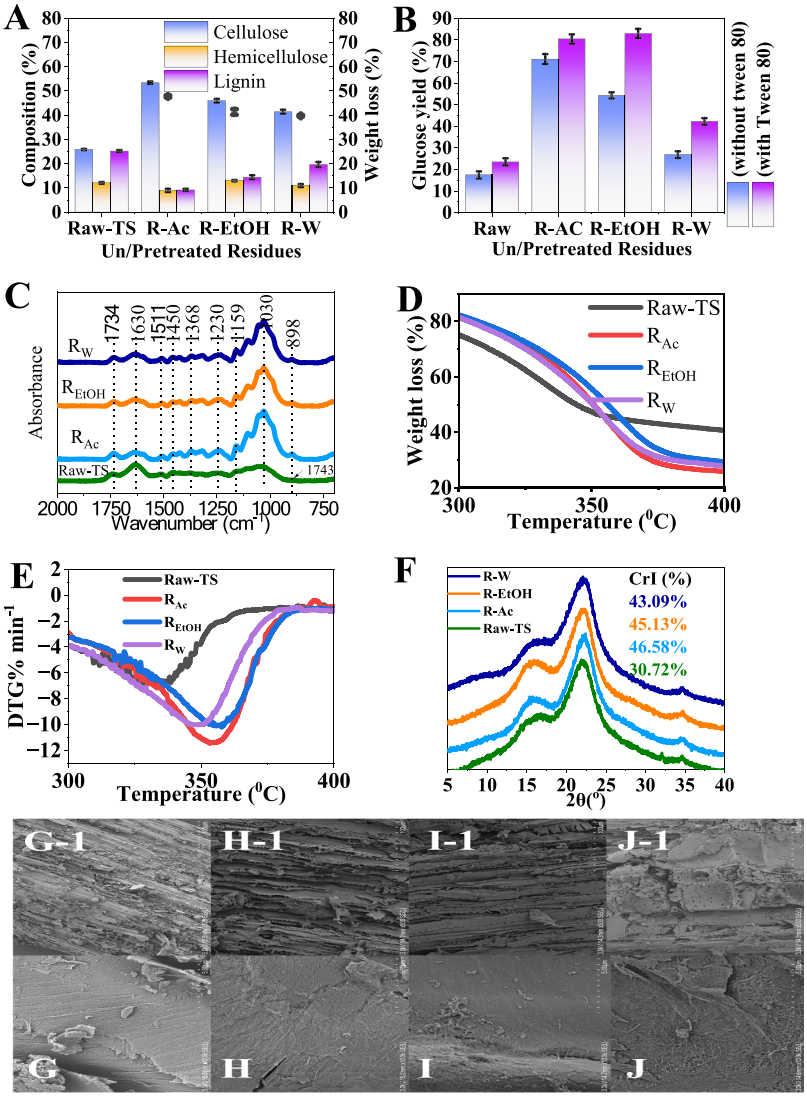


Figure 1. Characterization of untreated and pretreated TS residues: (A) Compositional analysis; (B) enzymatic hydrolysis yields of untreated and pretreated residues with and without T-80 addition; (C) FTIR spectra; (D) TGA thermograms; (E) DTG curves; (F) XRD patterns and corresponding crystallinity indices (CrI, %); and (G–J) SEM images revealing morphological characteristics (scale bars: 5 μm), with panels (G-1–J-1) showing the corresponding morphological characteristics at lower magnification (scale bars: 100 μm).

precipitation of hemicellulose imposes steric hindrance that further limits substrate accessibility during downstream utilization.[18] The severity of this redeposition is directly governed by solvent polarity; for instance, the introduction of a highly polar antisolvent like water rapidly decreases lignin solubility, forcing a dense, condensed aromatic layer (along with traces of hemicellulose, which might be linked to lignin as LCC) to coat the exposed carbohydrates. Consequently, this redeposited layer has potential to act as a primary sink for nonproductive cellulase adsorption via hydrophobic interactions (π-π) with the enzyme's binding modules and eventually possess the potential of limiting the EH yield.[14] Similarly, the incorporation of aqueous ethanol creates an intermediate polarity environment that can partially reduce lignin condensation but facilitates hemicellulose precipitation (along with traces of lignin, which might be linked to lignin via LCC), which yields a less dense redeposited layer (due to traces of lignin) and may result in better enzyme accessibility toward cellulose compared to pure water.[19] In contrast, the use of aqueous acetone enhances lignin solubility within the mixture, thereby preventing rapid lignin condensation; consequently, redeposition is inhibited, yielding a cleaner surface with increased disruption that is more suitable for the enzymatic hydrolysis process. Therefore, antisolvent selection is as critical as the DES pretreatment itself, directly dictating the efficiency of subsequent substrate valorization.

Considering the integrated biorefinery perspective, effective fractionation should combine efficient lignin recovery with preservation of a carbohydrate-rich residue that remains readily accessible to enzymatic hydrolysis. Among the tested antisolvents, 50% aqueous acetone provided the most favorable balance, yielding the highest lignin recovery (57.12%) and cellulose content (53.40%), the lowest residual lignin content (9.16%), and the highest subsequent EH yield (71.14%).

3.1.2. Enzymatic Digestibility of Pretreated Residues. Raw (Raw-TS) and pretreated residues (R-Ac, R-EtOH, and R-W) were subsequently subjected to EH, utilizing glucose yield

https://doi.org/10.1021/acssuschemeng.6c11956
ACS Sustainable Chem. Eng. XXXX, XXX, XXX–XXX

as a parameter for assessing structural disruption (Figure 1B). This evaluation aimed to elucidate the dynamic interplay between the structural disruption achieved during DES pretreatment and the subsequent surface deposition determining how these competing factors dictate the overall utilization of the pretreated residues.[20] Results revealed that R-Ac, R-EtOH, and R-W achieved EH yields of 71.14%, 54.29%, and 26.83%, respectively. This significant variation in EH yields despite identical pretreatment severity indicated the varying degrees of surface inhibition among the substrates.[18] This inhibitory effect was further investigated by the addition of T-80, which increased the EH yields for R-Ac, R-EtOH, and R-W to 80.46%, 83.02%, and 42.23%, respectively.[21] Interestingly, T-80 had a much stronger effect on R-EtOH, increasing the EH yield from 54.29% to 83.02%, while R-Ac increased from 71.14% to 80.46%. The lower initial digestibility of R-EtOH is consistent with its higher residual lignin and hemicellulose contents, which can increase surface inhibition through nonproductive cellulase adsorption and steric hindrance, respectively. By reducing lignin-associated interactions, T-80 likely increased the fraction of cellulase available for productive hydrolysis, resulting in the marked improvement observed for R-EtOH. In comparison, the smaller increase in R-Ac is consistent with its already higher enzymatic accessibility before surfactant addition. The pronounced response of R-EtOH to T-80 further suggests the presence of localized hydrophobic lignin-rich domains that favor nonproductive cellulase binding through hydrophobic and π−π interactions; competitive occupation of these sites by T-80 can therefore reduce enzyme sequestration and facilitate saccharification.[14] For R-W, however, the EH yield increased only to 42.23% after T-80 addition, suggesting that its recalcitrance was not governed solely by nonproductive enzyme adsorption. The extensive codeposition of lignin and other biomass components likely produced a dual-inhibitory effect by introducing nonproductive binding sites and forming a structural barrier that physically shields the underlying cellulose matrix. While T-80 can mitigate localized hydrophobic interactions, it cannot effectively overcome this steric barrier, explaining the persistently low EH yield of R-W after surfactant addition.[22,23]

3.1.3. Physicochemical Analysis of Un/Pretreated Residues. *3.1.3.1. FTIR Analysis of Un/pretreated Residues.* FTIR analysis was carried out to investigate the structural modifications in un/pretreated residues (Figure 1C). Specifically, the characteristic cellulose peaks at 1450, 1368, 1030, and 898 cm^{-1} were attributed to primary hydroxyl (−OH) bending at C6, methylene ($-CH_2-$) stretching, C−O pyranose ring stretching, and β-(1,4)-glycosidic linkages, respectively.[24] After the pretreatment, the relative intensities of absorption bands at 1030 and 898 cm^{-1} enhanced significantly, revealing a pronounced enrichment of carbohydrates in the pretreated residues. Conversely, the reduced intensity of the lignin absorption bands at 1630 and 1511 cm^{-1} indicated partial delignification, though their presence confirmed that residual lignin remained in the pretreated residues. Additionally, the 1743 cm^{-1} band, assigned to carbonyl (C═O) stretching, indicated the retention of hemicellulose. Following pretreatment, this unconjugated carbonyl band shifted from 1743 to 1734 cm^{-1}. This shift indicates the formation of stronger intermolecular hydrogen bonds, suggesting that upon the cleavage of native ester linkages, the residual carbonyl groups integrated into a tightly condensed electrostatic network. Interestingly, a comparison of the pretreated residues with the native biomass (Raw-TS) revealed a pronounced redshift in the broad hydroxyl stretching band, shifting from 3442 cm^{-1} in the Raw-TS to 3342 cm^{-1} among all pretreated residues. As H-bonding inherently shifts O−H stretching vibrations to lower wavenumbers, this pronounced redshift indicates a transition from sterically hindered, weakly interacting hydroxyls in the native matrix to a highly ordered, strongly interacting intermolecular hydrogen-bonding network following pretreatment.[25] While the redshift was consistently observed across all pretreated residues, the corresponding absorption band ratios were 0.017, 0.013, and 0.014 for R-Ac, R-EtOH, and R-W, respectively. These differences further suggest that antisolvent selection influences the local hydrogen-bonding environment of the recovered residues, while the ratios are interpreted comparatively rather than as absolute measures of H-bond strength.

3.1.3.2. TGA/DTG Analysis of Un/Pretreated Residues. TGA and DTG analyses were employed to evaluate the thermal degradation profiles of the untreated and pretreated residues (Figure 1D). Briefly, the native Raw-TS exhibited an early degradation shoulder (∼200−245 °C) indicative of hemicellulose decomposition, whereas its reduced contribution in the pretreated residues is consistent with substantial hemicellulose removal during DES pretreatment. Consequently, the shift of their degradation onsets to higher temperatures indicates the enrichment of a more thermally stable structural framework.[1]

Within the initial phase of degradation (∼300 °C), the rate of thermal decomposition accelerated in the order of R-W ≥ R-Ac > R-EtOH. The more rapid decomposition of R-W suggests a highly accessible and amorphous structure facilitating efficient heat transfer, whereas R-EtOH exhibited greater structural recalcitrance. However, approaching ∼350 °C, R-Ac began to degrade more rapidly than R-W, while R-EtOH maintained lower degradation rates. By ∼400 °C, the residual masses for R-Ac, R-EtOH, and R-W were 25.86%, 29.47%, and 27.92%, respectively, revealing R-Ac contains fewer recalcitrant domains than R-EtOH and R-W.

During the carbonization phase (400−700 °C), thermal degradation resulted in additional mass losses of 11.17%, 8.81%, and 11.81% for R-Ac, R-EtOH, and R-W, respectively. Consequently, the final char yields for these pretreated samples (14.69% for R-Ac, 19.11% for R-EtOH, and 17.66% for R-W) were substantially lower than that of the native Raw-TS (31.09%). Among the pretreated substrates, R-EtOH exhibited the highest char yield (19.11%), pointing to a more condensed and recalcitrant structure. Despite higher hemicellulose content in the R-EtOH, this enhanced thermal stability suggested that the coprecipitation of hemicellulose and lignin as LCC. Given that aqueous ethanol selectively precipitates LCCs, their resulting surface accumulation likely dictates the recalcitrance of R-EtOH by simultaneously imposing steric hindrance and providing active sites for nonproductive enzyme adsorption. In contrast, the recalcitrance of the R-W substrate results primarily from extensive lignin redeposition, which forms a continuous physical barrier over the exposed carbohydrates. The low char yield of R-Ac indicates high delignification efficiency and disruption of native cellulose crystallinity, confirming that aqueous acetone minimizes the surface redeposition of aromatic components.[20]

The DTG curves are consistent with these observations (Figure 1E). The broad, early degradation profile of Raw-TS (T_{max} ∼330 °C) shifted to higher temperatures post-pretreatment

https://doi.org/10.1021/acssuschemeng.6c11956
ACS Sustainable Chem. Eng. XXXX, XXX, XXX−XXX

(T_{max} = 348.41 °C for R-W, 354.15 °C for R-Ac, and 357.45 °C for R-EtOH), reflecting the removal of thermally labile hemicellulose. Relative to R-W, the R-Ac and R-EtOH residues displayed delayed and narrower degradation peaks, indicating a more uniform polymeric structure. The maximum thermal stability observed in R-EtOH (357.45 °C) is attributed to thermal shielding by its condensed residual lignin network.[18]

3.1.3.3. XRD Analysis of Residues. X-ray diffraction (XRD) was employed to evaluate the crystallinity index (CrI) of the native and pretreated residues (Figure 1F). The results exhibited characteristic peaks at 2θ ≈ 15°, 22°, and 34°, confirming the retention of the Cellulose I allomorph among all un/pretreated samples. Following DES pretreatment, the CrI increased from 30.72% in Raw-TS to 46.58%, 45.13%, and 43.09% for R-Ac, R-EtOH, and R-W, respectively. The overall increase in CrI following DES pretreatment is primarily attributed to the preferential removal of amorphous hemicellulose and lignin, thereby increasing the relative contribution of crystalline cellulose. The slightly lower CrI values of R-EtOH and R-W compared with R-Ac may reflect differences in the relative abundance of residual noncrystalline components within these residues. Considered alongside the compositional, SEM, and enzymatic hydrolysis results, these CrI differences are consistent with antisolvent-dependent variations in residue organization and substrate accessibility.[26,27]

3.1.3.4. Surface Morphology of Un/Pretreated Residues. The surface morphology of the native and pretreated residues was evaluated using SEM analysis as illustrated in Figure 1G−J. The untreated Raw-TS exhibited highly compact, closely packed architecture, reflecting the inherent physical recalcitrance of the intact LCB matrix. After the DES pretreatment, the pretreated residues exhibited rough surface topographies, visible macropores, extensive internal cracking, and structural disruption. The observed structural disruption was caused by lignin solubilization, which disrupts the structural integrity of biomass.

While pretreatment disrupted the LCB structure, the specific antisolvent dictated the localized reprecipitation dynamics. Compared to R-Ac (Figure 1H,H-1), the surface of the R-EtOH (Figure 1I,I-1) revealed irregular oligomeric agglomerations and condensed plaque-like structures along with spherical structures. Due to the relatively low polarity of ethanol, the lignin and LCCs underwent phase separation, forming a dense coating over the underlying cellulosic matrix upon precipitation. Conversely, the water-precipitated residue (R-W, Figure 1J,J-1) exhibited localized spherical deposits and heavily fused, web-like fibrillar networks. Induced by the rapid shift in polarity during aqueous dilution, the hydrophobic lignin macromolecules phase-separated and coalesced into discrete droplets, which subsequently redeposited onto the exposed cellulose, forming continuous physical barriers that restrict enzymatic accessibility.[28]

Collectively, the physicochemical analyses revealed a distinct antisolvent-dependent behavior in substrate structure and accessibility. Briefly, R-Ac exhibited the highest cellulose content, the lowest residual lignin content, and a more disrupted surface morphology, consistent with its higher EH. In contrast, R-EtOH retained more lignin and hemicellulose and showed greater surface agglomeration, while R-W exhibited the highest residual lignin content and the most extensive redeposited structures. These combined observations indicate that antisolvent-dependent redistribution of noncellulosic components strongly influences the final recalcitrance of the pretreated residues.

3.2. Antisolvent-Dependent Fractionation and Structural Characteristics of Recovered Lignin

L-Ac, L-EtOH, and L-W represented the lignin fractions recovered from the corresponding liquid streams and were characterized to evaluate the structural features of the recovered lignin.

3.2.1. FTIR Characterization of Native and Regenerated Lignin. FTIR spectroscopy was carried out to evaluate the structural modifications of native and isolated lignin fractions (Figure 2A). Absorption bands at 2931 and 2851 cm^{-1}, assigned to the C−H stretching vibrations of aliphatic methyl and methylene groups, were present in all samples. In the regenerated lignin, the characteristic aromatic skeletal vibrations in the regions of 1615−1630, 1512−1516, and 1460 cm^{-1} persisted, confirming the preservation of the core aromatic backbone following pretreatment.[4] However, the aromatic skeletal and conjugated carbonyl bands located at 1615 and 1512 cm^{-1} in the L-MWL shifted to 1630 and 1516 cm^{-1}, respectively, in the regenerated lignin samples. This shift toward a higher wavenumber is attributed to the disruption of the native intermolecular H-bonding network and the reduction of extended aromatic conjugation during depolymerization. Furthermore, the absorption bands assigned to syringyl (S, 1330 and 1230 cm^{-1}) and guaiacyl (G, 1267 and 1036 cm^{-1}) units, along with the aromatic C−O stretching vibration at 1118 cm^{-1}, were evaluated.[5] Interestingly, while these signals remained prominent in L-MWL and L-Ac, their intensities decreased in the L-EtOH and L-W fractions. This reduction suggests that polar antisolvents influence the selective fractionation and structural characteristics of the recovered lignin fractions. Consequently, the lower intensities of oxygen-containing and methoxyl-associated bands in L-EtOH and L-W indicate a structurally modified lignin fraction. Interestingly, the comparable signal intensities of L-MWL and L-Ac indicate greater preservation of these structural features in the acetone-recovered lignin, whereas the ethanol- and water-recovered fractions exhibited more pronounced structural alteration.

3.2.2. GPC Analysis. GPC analysis was used to determine the molecular weights of native and regenerated lignin fractions to investigate the structural modifications caused by antisolvents (Figure 2B). Briefly, L-MWL exhibited Mw of 26,845 Da and a Mn of 21,597 Da (PDI = 1.24), representing the inherent structure of lignin in TS. Following pretreatment, all extracted lignins underwent extensive depolymerization. The Mw values for L-Ac, L-W, and L-EtOH decreased to 6717, 6952, and 7087 Da, respectively, which, alongside corresponding Mn values of 6623, 6936, and 7010 Da, yielded a narrow PDI of 1.00−1.01 across all recovered fractions. Compared to L-MWL and L-Ac, the extensive depolymerization observed here suggests that the thiol (−SH) groups effectively scavenged reactive carbocations, preventing structural condensation and avoiding the typical acid-catalyzed repolymerization. The slight increase in Mw observed for L-W and L-EtOH, compared to L-Ac, indicates that the polarity of the antisolvent influences the selective fractionation, leading to the recovery of slightly higher molecular weight lignin.[4]

Briefly, Figure 2C illustrates the proposed lignin protection mechanism, wherein the solvent acts as a stabilizing nucleophile due to the presence of the thiol group. This moiety impedes undesirable electrophilic aromatic substitution by intercepting the reactive Cα carbocations generated during β−O−4 cleavage, thereby preventing unwanted C−C bond formation and suppressing lignin condensation.[1]

https://doi.org/10.1021/acssuschemeng.6c11956
ACS Sustainable Chem. Eng. XXXX, XXX, XXX−XXX

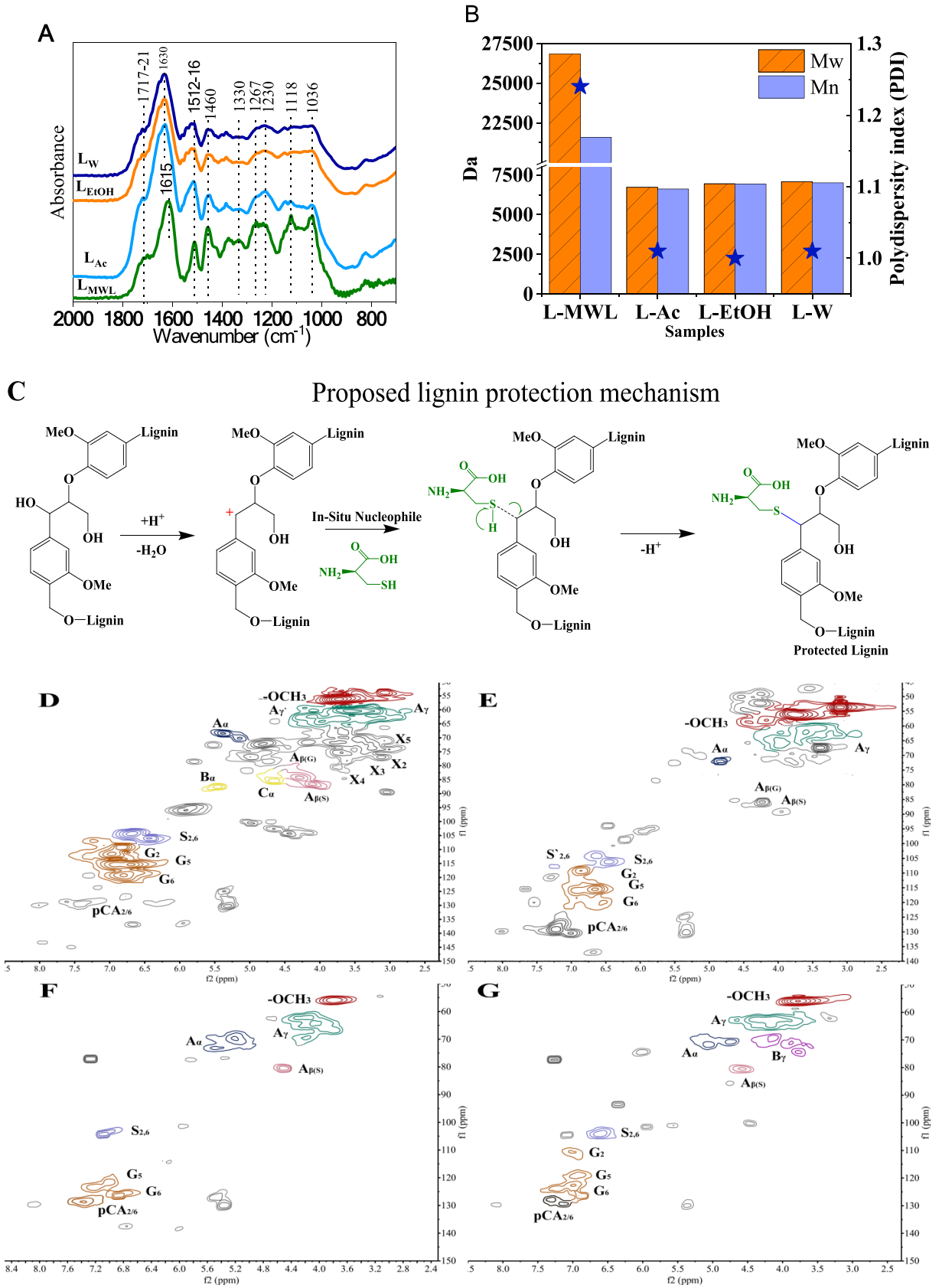


Figure 2. Structural characterization of regenerated lignin obtained using different dilution agents. (A) FTIR spectra of regenerated lignin; (B) weight-average (Mw) and number-average (Mn) molecular weights, along with the corresponding polydispersity index (PDI); (C) proposed lignin protection pathway; (D) 2D-HSQC NMR spectra, where L-MWL (D) represents milled wood lignin extracted from TS (control), while L-Ac (E), L-EtOH (F), and L-W (G) denote lignin regenerated after dilution with the corresponding reagents.

https://doi.org/10.1021/acssuschemeng.6c11956
ACS Sustainable Chem. Eng. XXXX, XXX, XXX−XXX

3.2.3. 2D-NMR (HSQC) of Native and Regenerated Lignin. The structural characteristics of the native and regenerated lignin fractions were evaluated using 2D HSQC NMR spectroscopy (Figure 2D−G). Briefly, L-MWL served as the control to investigate the structural modifications induced by the different antisolvent treatments. In the side-chain region (δ_C/δ_H 48−90/2.50−5.80 ppm), L-MWL displayed prominent correlations for β-O-4 (A), β−5 (B), and β-β (C) substructures, with β-O-4 linkages predominating.[20,29−31] Results indicated that L-MWL and L-Ac exhibited significantly higher methoxyl ($-OCH_3$) signal intensities compared with L-EtOH and L-W, suggesting a higher methoxyl content in the acetone-extracted fractions. Moreover, L-MWL exhibited 30.18% β-O-4, 12.34% β−5, and 7.14% β-β linkages, alongside residual carbohydrate signals (X_2−X_5), consistent with native lignin preparations. The regenerated lignins (L-Ac, L-EtOH, and L-W) showed 19.67%, 33.14%, and 30.07% β-O-4 retention, respectively. The L-Ac spectrum exhibited the retention of both Aβ(G) and Aβ(S) signals, whereas L-EtOH and L-W displayed only Aβ(S) correlations. The disappearance of Aβ(G) signals in the L-EtOH and L-W suggests that G units are more susceptible to condensation than S units, due to the unsubstituted C5 position on the G ring under the aqueous ethanol and water environment.[4]

The aromatic region (δ_C/δ_H 100−150/5.0−8.0 ppm) of L-MWL and L-Ac exhibited strong S and G unit correlations, confirming the preservation of the aromatic backbone of lignin. In contrast, L-EtOH and L-W showed reduced signal intensity reflecting structural condensation induced by polar antisolvents, which might have caused chain mobility restrictions and eventually reduced vibrational freedom. The G_2 signal, observed in L-MWL and L-Ac, was absent in L-EtOH and weak in L-W. The marked reduction in the G_2 correlation observed for L-EtOH, together with its lower intensity in L-W relative to L-MWL and L-Ac, indicates a greater degree of structural condensation within these recovered lignin fractions, consistent with an increased contribution of C−C interunit linkages. These observations are inline with the FTIR data, which showed reduced absorption band for S and G units in the L-EtOH and L-W fractions. The p-coumarate (pCA) structure (δ_C/δ_H 128.94/7.19 ppm) remained preserved in all samples, with L-Ac exhibiting the highest correlation intensity, confirming the relative stability of this moiety during fractionation. These structural observations further demonstrate that antisolvent selection influences the selective fractionation of dissolved lignin during recovery. The higher recovery of L-Ac relative to L-EtOH and L-W, together with the higher residual lignin contents of R-EtOH and R-W, is consistent with greater retention of lignin within the corresponding recovered residues. Such antisolvent-dependent lignin distribution ultimately influences both lignin recovery and downstream substrate valorization.[32]

3.3. Antisolvent-Induced Hydrophobic Domains Drive Nonproductive Enzyme Adsorption

3.3.1. QCM-D Kinetic Analysis of Substrate Surface Structure and Enzymatic Hydrolysis of Pretreated Residues. QCM-D has been used to investigate the interaction between enzymes and substrate/lignin. Therefore, the residues after different dilution solvents are subjected to QCM-D to investigate the interaction between residues and enzymes (Figure 3A).[14] The holocellulose control (R-HC) exhibited the highest digestibility, yielding a shift of 100.29 Hz, which corresponds to a total mass removal of 1775.13 ng/cm^2. Among the DES pretreated substrates, the R-Ac demonstrated higher hydrolysis efficiency, achieving a mass removal of 979.52 ng/cm^2 (at a maximum shift of 55.34 Hz). In contrast, R-EtOH and R-W exhibited severely restricted hydrolysis kinetics, digesting only 422.68 ng/cm^2 (23.88 Hz) for R-EtOH and 207.27 ng/cm^2 (11.71 Hz) for R-W.

Lignin structure is considered the primary factor limiting EH; however, the residual lignin within the R-Ac substrate exhibited the least nonproductive cellulase adsorption. By limiting the irreversible nonproductive enzyme adsorption onto lignin, a larger fraction of the bulk enzymes remained available for cellulose hydrolysis. Other than R-HC, the enhanced digestibility of the R-Ac substrate represents the structural characteristics of this residue and the residual lignin present in favor of EH. These results indicate that aqueous acetone dilution did not cause (much) lignin precipitation; consequently, the disrupted pretreated residue remained more accessible for EH compared to the highly recalcitrant R-EtOH and R-W residues.[1] The severe recalcitrance observed in the R-EtOH and R-W substrates is attributed to the presence of highly hydrophobic, condensed lignin or LCC domains. These structural variations are driven by the distinct phase dynamics between the varying precipitation antisolvents and the DES. Ultimately, these reprecipitated domains (structurally composed of condensed lignin, LCCs or hemicellulose) act as structural barriers that have potential to irreversibly bind enzymes, drive nonproductive enzyme adsorption, and eventually limit the overall hydrolysis.[19,33]

High-resolution evaluation of the transient phase following enzyme injection provides quantitative insight into the competing dynamics between productive cellulose hydrolysis and nonproductive enzyme adsorption, which was directly related to the structure of residues (Figure 3B−F). It has been reported that the residual lignin limits enzymatic efficiency by acting simultaneously as a steric barrier and an enzyme adsorption sink.[34] The holocellulose control (R-HC) defined the baseline for the uninhibited catalytic activity of enzymes, revealing a rapid transition to bulk hydrolysis (Δt = 30.91 s) and a high initial hydrolysis velocity (V_0 = 0.072 Hz/s) after an initial enzyme mass adsorption of 90.62 ng/cm^2. Comparatively, the R-Ac also exhibited almost similar behavior as R-HC. Briefly, R-Ac exhibited the shortest transition period (Δt = 28.41 s), a lower initial enzyme adsorption mass of 74.69 ng/cm^2, and an initial hydrolysis velocity of V_0 = 0.066 Hz/s. The minimal mass accumulation (74.69 ng/cm^2) and rapid onset of hydrolysis suggest that the residual lignin structure in R-Ac allows cellulases to bypass nonproductive binding sites and directly hydrolyze the cellulose chains (Figure 3G). In contrast, the kinetic profile of the R-EtOH demonstrates the competitive adsorption sink effect. R-EtOH exhibited the highest initial mass adsorption (100.89 ng/cm^2) and extended transition time (Δt = 59.16 s) to initiate hydrolysis with a reduced initial hydrolysis velocity (V_0 = 0.041 Hz/s) (Figure 3H). The higher initial hydrolysis velocity of R-Ac is consistent with its lower residual lignin content and higher cellulose content (Figure 1A), which provide a more accessible substrate surface for productive enzymatic hydrolysis, whereas the higher lignin and hemicellulose contents of R-EtOH increase surface inhibition and restrict enzyme access to cellulose. This behavior indicates that the residual lignin/LCCs present in the R-EtOH rapidly and unproductively bind a large fraction of the available enzymes via their hydrophobic domains prior to hydrolysis. Furthermore, the R-W exhibited severe kinetic

https://doi.org/10.1021/acssuschemeng.6c11956
ACS Sustainable Chem. Eng. XXXX, XXX, XXX−XXX

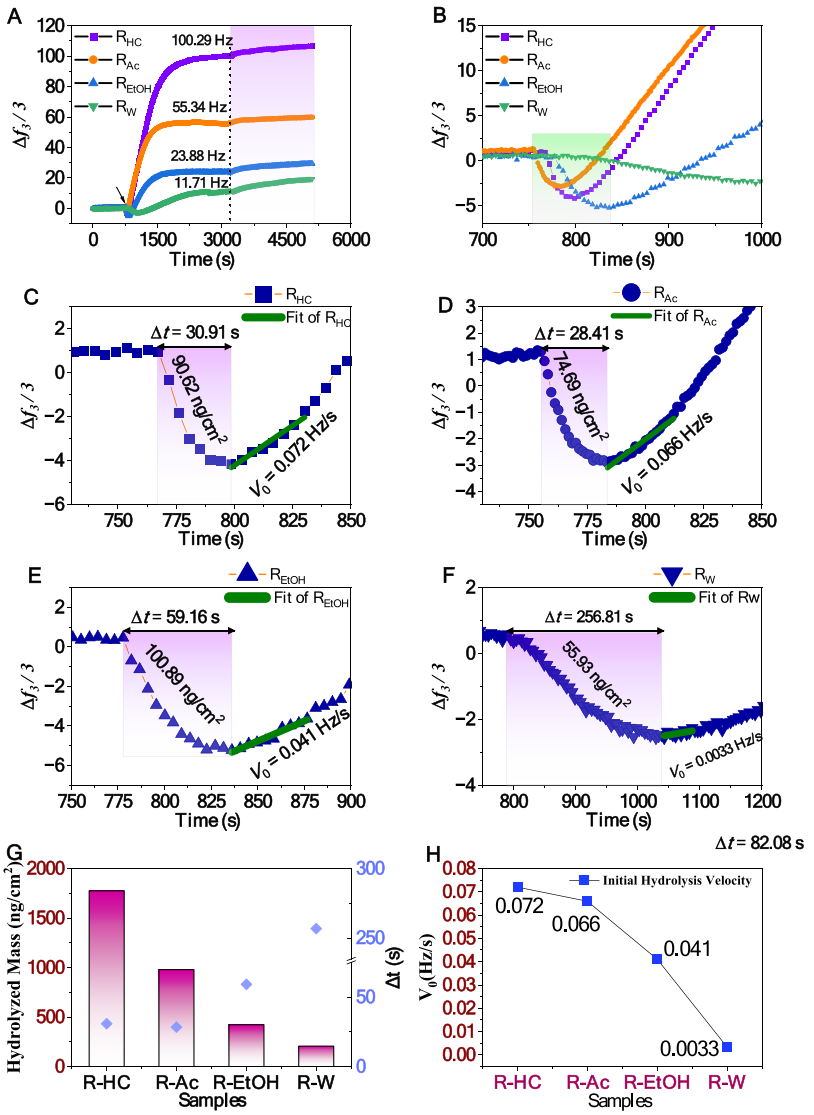


Figure 3. Quartz crystal microbalance (QCM) sensograms monitoring EH; upon injecting enzymes on holocellulose and pretreated substrates. (A) Normalized frequency shift ($\Delta f_3/3$) over the full monitoring period for R-HC, R-Ac, R-EtOH, and R-W; (B) Magnified portion of the frequency response during the initial enzyme−substrate interaction window, highlighting the differences among samples; (C−F) individual frequency-shift profiles with linear fitting for R-HC, R-Ac, R EtOH, and R-W, respectively, showing the reaction time interval (Δt), corresponding adsorbed mass, and initial hydrolysis velocity (V_0); (G) hydrolyzed mass and reaction time (Δt) for sample; (H) initial hydrolysis velocity (V_0) among samples.

inhibition, evidenced by an extended transition delay (Δt = 256.81 s), a low initial adsorption of 55.93 ng/cm^2, and a negligible initial velocity (V_0 = 0.0033 Hz/s). This delayed kinetic response indicates that the R-W surface acts as a substantial structural and chemical barrier, restricting initial enzyme access to the underlying carbohydrate. Consequently, these transient kinetic profiles confirm that solvent-specific lignin precipitation directly dictates the physicochemical barrier properties of the residual biomass.

3.3.2. Mechanistic Insights into Cellulase-Lignin Adsorption Kinetics and Binding Reversibility. To determine whether the residue-level QCM-D behavior was associated with the lignin remaining within the pretreated substrates, residual lignin was extracted directly from R-Ac, R-EtOH, and R-W and designated as R-L$_{Ac}$, R-L$_{EtOH}$, and R-L$_W$, respectively. These residue-derived lignins were evaluated independently to relate their cellulase-binding characteristics to the interfacial behavior observed for the corresponding whole-residue films (Figure 4A−E). Briefly, L$_{MWL}$ exhibited the highest maximum cellulase adsorption capacity at 536.31 ng/cm^2 (Δf = −30.30 Hz), of which 401.79 ng/cm^2 remained irreversibly bound after buffer rinsing (−22.70 Hz). The extracted lignin fractions from the residues obtained after the differently diluted reagents (R-L$_{Ac}$, R-L$_{EtOH}$, and R-L$_W$) demonstrated a notably reduced initial binding capacity, reaching maximum adsorbed masses between 418.43 and 423.92 ng/cm^2. This overall reduction is consistent with previous findings demonstrating that certain extractable lignin fractions possess lower maximum enzyme adsorption capacities than native lignin, thereby mitigating nonproductive binding.[23]

During the desorption phase, pronounced differences in cellulase retention and binding reversibility were observed among the residual lignin fractions. Although the R-L$_{AC}$ and R-L$_{EtOH}$ lignins reached an identical maximum adsorption mass of

https://doi.org/10.1021/acssuschemeng.6c11956
ACS Sustainable Chem. Eng. XXXX, XXX, XXX−XXX

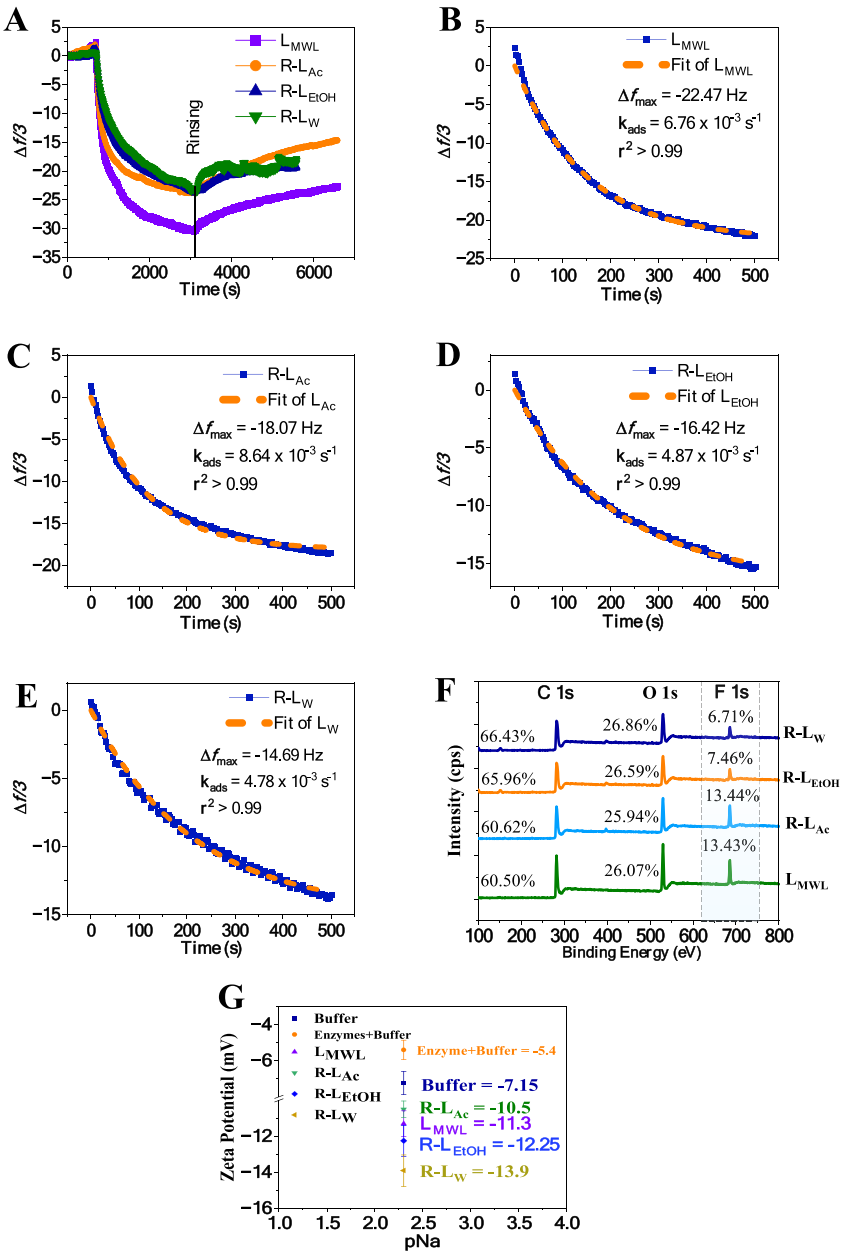


Figure 4. QCM-D analysis of enzyme adsorption behavior on the lignin extracted from the pretreated residues and compared with L-MWL, together with surface elemental composition and surface charge characteristics. (A) Normalized frequency shift ($\Delta f/3$) as a function of time for L-MWL, R-L-Ac, R-L-EtOH, and R-L-W before and after rinsing; (B–E) individual frequency-shift profiles with corresponding kinetic fitting for L-MWL, R-L-Ac, R-L-EtOH, and R-L-W, respectively, showing the maximum frequency shift (Δf_{max}), adsorption rate constant (k_{ads}), and coefficient of determination (r^2); (F) XPS survey spectra of L-MWL, R-L-Ac, R-L-EtOH, and R-L-W, with corresponding atomic percentages of C 1s, O 1s, and F 1s; (G) zeta potential of all components involved in QCM analysis as a function of sodium ion strength (pNa).

~423.92 ng/cm^2, their respective affinities for the enzyme desorption differed considerably. The R-L$_{EtOH}$ fraction exhibited an 81.00% irreversibility rate, permanently retaining 343.38 ng/cm^2 (−19.52 Hz) of the enzyme. Conversely, the R-L$_{AC}$ fraction demonstrated the highest desorption efficiency at 38.71%, retaining an irreversible mass of only 259.84 ng/cm^2 (Δf = −14.68 Hz). The R-L$_W$ displayed an intermediate irreversibility of 78.09% (326.74 ng/cm^2). It has been reported that the cellulase binding affinity is highly dependent on specific structural features of the substrate, such as the syringyl-to-guaiacyl (S/G) ratio and the distribution of hydrophobic structure.[35] The distinct reversibility observed on the R-L$_{AC}$ suggests that aqueous acetone dilution did not cause the reprecipitation of lignin; instead, it yielded a pretreated residue with a higher delignification, and the structure of this residual lignin is favorable for EH. These results are inline with the already reported literature, where residual lignin showed a positive impact toward EH by reducing nonproductive enzyme binding.[23]

To further elucidate the binding mechanics driving these interactions, the initial rapid adsorption phase (0–500 s) was evaluated to determine the kinetic rate constants (k_{ads}) (Table 1). Evaluating the rate constants indicates an inverse

https://doi.org/10.1021/acssuschemeng.6c11956
ACS Sustainable Chem. Eng. XXXX, XXX, XXX−XXX

Table 1. QCM-D-Derived Adsorption and Desorption Kinetic Parameters for Lignin-Enzyme Interactions Across Lignins Extracted from Various Pretreated Residues (L-MWL (control), R-LAC, R-LEtOH, R-LW), Including Adsorbed Mass, Irreversibly Bound Mass, Desorption Efficiency, Irreversibility (%), and Adsorption Rate

lignin sample	$\Delta f/3$ (Hz)	adsorbed mass (ng/cm^2)	post-rinse $\Delta f/3$ (Hz)	irreversible mass (ng/cm^2)	desorption efficiency (%)	irreversibility (%)	k_{ads} (x10^{-3})
L-MWL	−30.30	536.31	−22.70	401.79	25.08%	74.92%	6.76
R-L$_{Ac}$	−23.95	423.92	−14.68	259.84	38.71%	61.29%	8.64
R-L$_{EtOH}$	−23.95	423.92	−19.52	343.38	19.00%	81.00%	4.87
R-L$_{W}$	−23.64	418.43	−18.46	326.74	21.91%	78.09%	4.78

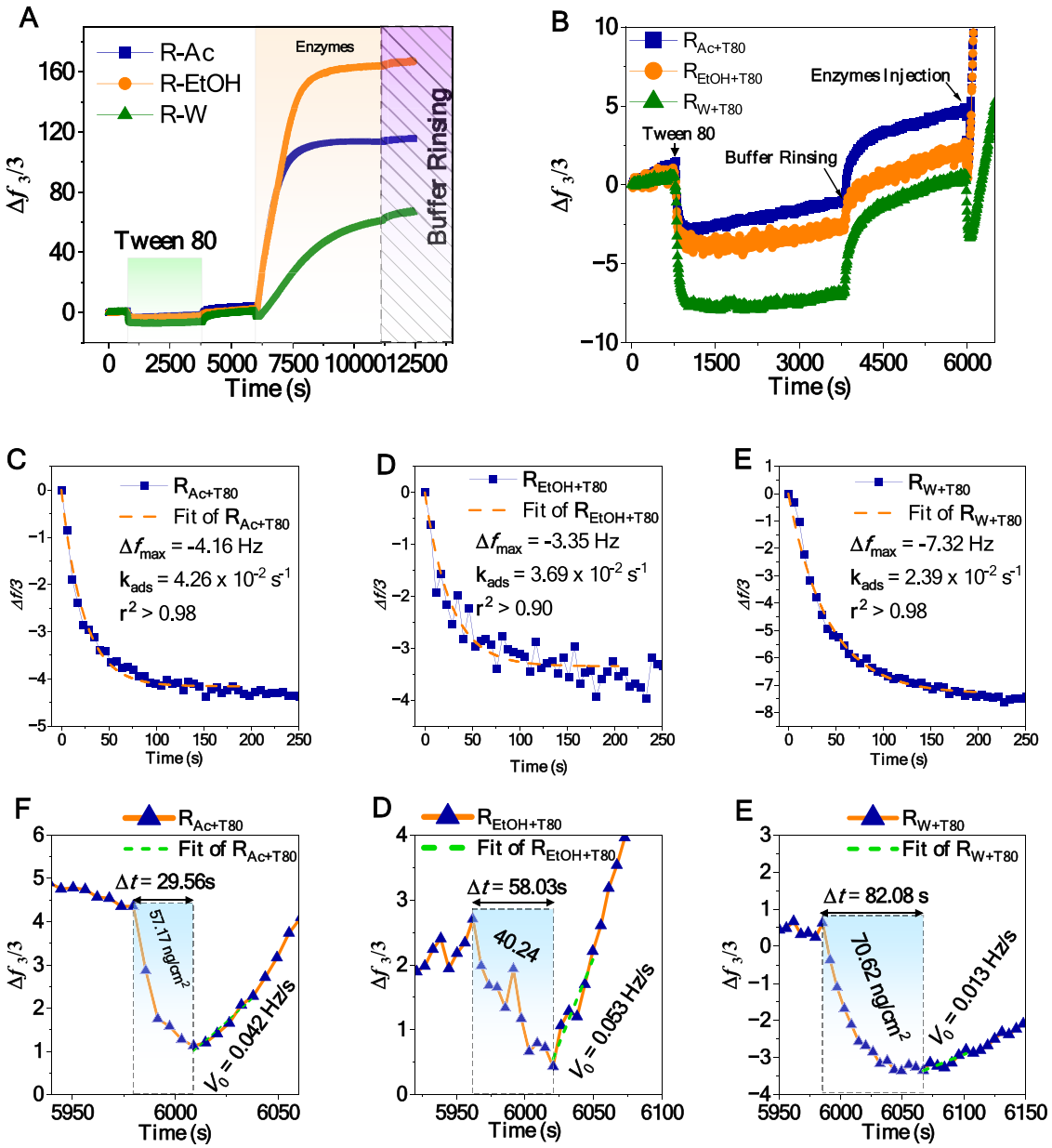


Figure 5. Effect of T-80 on the enzymatic hydrolysis (EH) of pretreated residues monitored by QCM. (A) Frequency shift ($\Delta f_3/3$) for R-Ac, R-EtOH, and R-W, showing T-80 addition, enzyme injection, and buffer rinsing; (B) magnified view of panel (A), highlighting the difference in frequency shift ($\Delta f_3/3$) for R-Ac + T80, R-EtOH + T80, and R-W + T80; (C−E) frequency-shift profiles corresponding to the rate of T80 adsorption on the pretreated residues for R-Ac + T80, R-EtOH + T80, and R-W + T80, along with rate of adsorption (k_{ads}) representing the T80 adsorption on pretreated residues, and r^2 values indicating the goodness of fit; (F−H) kinetic fitting of the pretreated samples evaluating their behavior upon enzyme injection, showing the maximum frequency shift (Δf_{max}) caused by enzyme adsorption, mass adsorbed on it, and initial hydrolysis velocity (V_0) along with response time (Δt) to start hydrolysis.

https://doi.org/10.1021/acssuschemeng.6c11956
ACS Sustainable Chem. Eng. XXXX, XXX, XXX−XXX

correlation between the initial adsorption velocity and the final binding irreversibility. The R-L_{Ac} fraction recorded the highest adsorption rate (8.64×10^{-3} s^{-1}), exceeding the native L-MWL control (6.76×10^{-3} s^{-1}). In conjunction with the previously observed high desorption efficiency for R-L_{Ac}, this rapid kinetic profile suggests that precipitation in aqueous acetone yields a surface with highly accessible binding sites. These sites likely promote rapid, reversible enzyme attachment dominated by weak electrostatic or H-bonding interactions rather than stable hydrophobic interaction. In contrast, the R-L_{EtOH} and R-L_W fractions presented the lowest adsorption rates, with k_{ads} values of 4.87×10^{-3} and 4.78×10^{-3} s^{-1}, respectively. For the R-L_{EtOH} fraction, this slower adsorption phase, together with its high irreversible mass retention, points to a time-dependent mechanism. The data indicates that the cellulases undergo a slower conformational rearrangement upon initial surface contact, requiring extended time to establish the permanent hydrophobic interactions characteristic of the R-L_{EtOH} substrate.

The native L-MWL presents a highly heterogeneous surface with a dense network of diverse polar and hydrophobic binding sites, enabling its maximum overall capacity for enzyme adsorption.[23] The rapid, reversible binding on the R-L_{Ac} surface suggests a predominantly hydrophilic character, likely enriched in polar functional groups or syringyl units that lack the extended aromatic domains required for permanent hydrophobic binding. Conversely, the delayed but highly irreversible adsorption on the R-L_{EtOH} surface indicates a chemically rigid and highly hydrophobic architecture that restricts immediate enzyme attachment but subsequently promotes stable, irreversible enzyme binding. The intermediate recovery of the R-L_W fraction points to a surface where intense hydrophobic segments are partially buried due to precipitation in a highly polar aqueous environment, restricting initial enzyme access while forming slightly less rigid complexes than the ethanol precipitate.

3.3.2.1. XPS and Zeta Potential of Extracted Lignin from Pretreated Residues. To gain further insights into the lignin-cellulase interfacial interactions, XPS analysis of chemically derivatized lignin samples was employed to quantify the surface −OH groups and correlate these structural characteristics with the binding dynamics observed via QCM-D (Figure 4F).[16,36] Results revealed that the R-L_{Ac} exhibited an atomic fluorine (F) content of ∼13% and a carbon content of ∼60%, values that are identical to those of the native-like L-MWL. This indicates that the R-L_{Ac} substrate retained a high concentration of accessible surface −OH groups.

In contrast, precipitation in alternative antisolvents induced severe structural condensation and the substantial depletion of these critical −OH groups. Results revealed remarkably lower F contents for the R-L_{EtOH} (7.46%) and R-L_W (6.71%) substrates, accompanied by elevated carbon densities of 65.96% and 66%, respectively. It indicates that the loss of such polar functional groups potentially yields a carbon-dense structure dominated by hydrophobic domains. As demonstrated by the QCM-D measurements, these highly hydrophobic surfaces are directly responsible for the severe recalcitrance of these substrates.[14]

Moreover, to evaluate the interfacial forces governing enzyme−substrate interactions, the zeta potential of the isolated lignins (R-L_{Ac}, R-L_{EtOH}, and R-L_W) and the cellulase mixture were measured at the hydrolysis pH (4.8) (Figure 4G). Briefly, the cellulase enzymes exhibited a net anionic potential of −5.78 mV. Similarly, all lignin preparations displayed negative surface charges, establishing a baseline electrostatic double-layer repulsion between the macromolecules. The L-MWL recorded a potential of −11.3 mV. R-L_{Ac} demonstrated a comparable potential of −10.5 mV, suggesting that the acetone antisolvent preserves a near-native electrostatic profile without inducing extensive surface modifications. In contrast, the lignin extracted from the water- and ethanol-diluted residues exhibited a more pronounced anionic surface charge, yielding potentials of −13.9 mV (R-L_W) and −12.25 mV (R-L_{EtOH}), respectively.

Based on the principle of colloidal electrostatics, these strongly electronegative surfaces would be expected to exert maximal repulsive forces against anionic cellulases, theoretically minimizing enzyme adsorption.[15] However, the transient QCM-D kinetics demonstrated the inverse behavior, revealing extensive, irreversible enzyme binding onto both the R-L_W and R-L_{EtOH} matrices. This apparent electrostatic contradiction confirms that nonproductive adsorption on these pretreated substrates is predominantly driven by hydrophobic forces instead of electrostatic forces. This apparent electrostatic contradiction indicates that nonproductive adsorption on these pretreated substrates is predominantly associated with hydrophobic interactions rather than electrostatic forces. The localized hydrophobic domains generated during water and aqueous ethanol precipitation can therefore overcome the electrostatic repulsion between the negatively charged lignin surfaces and cellulase, contributing to the irreversible, nonproductive enzyme adsorption observed for these pretreated substrates.[22]

3.3.3. Competitive Surfactant Adsorption Neutralizes Lignin-Derived Hydrophobic Sinks. To further investigate the role of residual lignin in nonproductive enzyme adsorption, T-80 was employed as a surfactant probe to assess the extent to which these interactions could be reduced (Figure 5A−H). Briefly, R-Ac (Figure 5A,C) yielded the fastest initial T80 adsorption rate ($k_{ads,T80} = 4.26 \times 10^{-2}$ s^{-1}) but recorded the lowest maximum T80 adsorption (53.10 ng/cm^2, corresponding to a frequency shift of −3.0 Hz and the lowest binding irreversibility (73.3%, retaining 38.94 ng/cm^2). This rapid kinetic response combined with a low total capacity of T80 adsorption confirms that the precipitation in 50% aqueous acetone yields a predominantly hydrophilic surface where hydrophobic sites are exposed but quantitatively minimal, lacking the dense networks required to permanently bind the T80 surfactant. The limited hydrophobic capacity of the R-Ac substrate directly correlates with its lower affinity for nonproductive cellulase binding and its higher saccharification efficiency. In contrast, the R-EtOH exhibited a moderately slower adsorption rate ($k_{ads,T80} = 3.70 \times 10^{-2}$ s^{-1}) alongside a higher total adsorbed mass of 76.11 ng/cm^2 (−4.3 Hz) (Figure 5A,D). Furthermore, R-EtOH demonstrated the highest binding irreversibility at 83.7% (63.72 ng/cm^2 retained). This elevated retention rate, and T80 adsorption (compared to R-Ac) suggests that the hydrophobic domains on the R-EtOH surface are highly condensed, forming rigid, irreversible interactions with the surfactant upon binding. Finally, the water-precipitated residue (R-W) recorded the slowest initial adsorption rate ($k_{ads,T80} = 2.39 \times 10^{-2}$ s^{-1}) yet exhibited the highest maximum T80 adsorption capacity at 138.06 ng/cm^2 (−7.8 Hz), retaining 109.74 ng/cm^2 of surfactant after buffer rinsing (79.5% irreversibility) (Figure 5A,E). The inverse relationship between the slow kinetic binding rate and the high total adsorption capacity indicates initial diffusional resistance into a matrix that possesses the largest total volume of available hydrophobic binding sites. This extensive hydrophobic sink accounts for the

https://doi.org/10.1021/acssuschemeng.6c11956
ACS Sustainable Chem. Eng. XXXX, XXX, XXX−XXX

severe kinetic suppression observed during the baseline enzymatic hydrolysis of R-W.

To elucidate the transient enzyme−substrate dynamics following surfactant modification, the initial kinetic phase immediately after cellulase injection was evaluated for the T80-treated residues (Table 2). It is important to mention that $k_{ads,T80}$ represents T-80 adsorption onto the pretreated residue, whereas initial hydrolysis velocity (V_0) reflects the initial rate of enzyme-mediated substrate mass removal; thus, the two parameters represent distinct interfacial processes. Analysis of the transition time delay (Δt), initial enzyme adsorption mass, and V_0 confirmed that competitive surfactant adsorption successfully mitigated nonproductive binding, particularly on the highly condensed hydrophobic surfaces (Figure 5F−H). The ethanol-precipitated residue (R-EtOH + T80) demonstrated the most significant mechanistic shift. Following T80 treatment, the initial unproductively adsorbed enzyme mass on R-EtOH was restricted to 40.24 ng/cm^2, enabling the highest V_0 = 0.053 Hz/s among the treated samples with a Δt = 58.03 s. These findings demonstrate that T80 effectively occupied the highly hydrophobic lignin domains, neutralizing the previously observed enzyme sink effect and allowing the bulk of the cellulase to engage directly in productive hydrolysis. The acetone-precipitated residue (R-Ac + T80) maintained the shortest transition time (29.56 s) with an initial adsorbed mass of 57.17 ng/cm^2 and a V_0 = 0.042 Hz/s, consistent with its inherently hydrophilic surface that required minimal surfactant remediation. As supported by the XPS analysis, this preservation of polar functionalities directly corresponds with its reduced hydrophobic capacity. Consequently, the presence of these hydroxyl groups effectively mitigates nonproductive enzyme binding by providing a hydrophilic barrier against permanent hydrophobic attachment.

Conversely, while the water-precipitated residue (R-W + T80) showed improved kinetics compared to its severely recalcitrant untreated baseline, it still recorded the longest transition delay (82.08 s), the highest initial enzyme adsorption mass (70.62 ng/cm^2), and the lowest V_0 = 0.013 Hz/s among the treated samples. This suggests that while T80 successfully blocked superficial hydrophobic sites, the highly condensed R-W matrix still presents considerable steric hindrance and residual nonproductive binding capacity. Overall, these transient profiles physically validate that occupying hydrophobic lignin domains with nonionic surfactants directly reduces nonproductive enzyme sequestration and accelerates the onset of active cellulose depolymerization. Ultimately, integrating these findings elucidates that the quantitative depletion of surface −OH groups shifts the dominant interfacial forces from reversible H-bonding to rigid hydrophobic interactions. This shift creates the robust hydrophobic sinks and highly condensed surfaces responsible for the extensive surfactant adsorption, prolonged transition delays, and permanent enzyme binding irreversibility observed in the R-W and R-EtOH residues, thereby promoting the nonproductive adsorption of cellulases.

3.4. Discussion

Following DES pretreatment, antisolvent addition is widely employed to reduce solvent viscosity and facilitate solid−liquid separation during DES recovery.[12,13,37] However, the effect of antisolvent selection on the physicochemical properties, structural accessibility, and downstream valorization of the recovered biomass remains insufficiently understood. Treating these media as inert washing agents overlooks the distinct solvent environments established during dilution and their potential influence on component redistribution. Although different antisolvents have been employed in DES fractionation studies, their recovery-stage effects are commonly embedded within broader pretreatment protocols rather than evaluated independently under otherwise identical pretreatment conditions (Table 3).[17,38−41] In contrast, our results demonstrate that antisolvent selection substantially influences substrate recalcitrance and the characteristics of the recovered lignin (Table 3), which directly impacts the overall resource utilization and fractionation efficiency of the process.

During DES recovery, antisolvent selection alters the solvent environment at the point of separation and consequently influences the distribution of dissolved lignin, carbohydrates, and LCC-derived components between the liquid and recovered solid fractions. In the aqueous-acetone system, the higher lignin recovery and lower residual lignin content are consistent with greater retention of solubilized lignin within the liquid fraction during dilution. The recovered L-Ac fraction exhibited a β-O-4 content of 19.67%, further indicating selective structural fractionation of the solubilized lignin. The resulting residue presented an accessible surface, confirmed by the shortest QCM-D transition to hydrolysis. Together, these properties accounted for their considerably high glucose yield and limited nonproductive enzyme binding.[42] In the context of sustainable biomass processing, this indicates that aqueous acetone effectively enables the conversion of a waste matrix into high-value

Table 2. QCM-Derived Kinetic Parameters for Surfactant (T-80) Adsorption onto Pretreated Residues (R-AC, R-EtOH, R-W) and Subsequent Enzyme−Substrate Binding Dynamics on T80-Treated Residues[a]

surfactant (T-80) adsorption kinetics (pretreated residues)			
	r-Ac	R-EtOH	R-W
max T80 adsorption capacity	53.10 ng/cm^2 (−3.0 Hz)	76.11 ng/cm^2 (−4.3 Hz)	138.06 ng/cm^2 (−7.8 Hz)
binding irreversibility	73.3%	83.7%	79.5%
retained T80 mass	38.94 ng/cm^2	63.72 ng/cm^2	109.74 ng/cm^2
initial adsorption rate ($k_{ads,\ T80}$)	4.26 × 10^{-2} s^{-1}	3.70 × 10^{-2} s^{-1}	2.39 × 10^{-2} s^{-1}
enzyme-substrate dynamics (T80-treated residues)			
transition time delay (Δt)	29.56 s	58.03 s	82.08 s
initial adsorbed enzyme mass	57.17 ng/cm^2	40.24 ng/cm^2	70.62 ng/cm^2
initial enzyme mediated hydrolysis velocity (V_0)	0.042 Hz/s	0.053 Hz/s	0.013 Hz/s

[a]Analyzed parameters include initial adsorption rate, maximum adsorption capacity, binding irreversibility, retained surfactant mass, transition delay time, initial enzyme adsorbed mass, and initial hydrolysis velocity.

https://doi.org/10.1021/acssuschemeng.6c11956
ACS Sustainable Chem. Eng. XXXX, XXX, XXX−XXX

Table 3. Overview of Antisolvent-Assisted Post-Pretreatment Separation in DES-Mediated Biomass Fractionation, Including Dilution Media and Their Reported Effects on Different Lignocellulosic Feedstocks

DES	recovery method	dilution agent	biomass	effect	ref
ChCl + LA	antisolvent	water	rice straw	~60% delignification	44
ChCl + LA + ethanol	antisolvent	ethanol	*Broussonetia papyrifera*	glucose yield increased by ~130%, 86.71% xylan content decreased	45
ChCl + LA ChCl + oxalic acid (OA)	antisolvent	absolute ethanol	bagasse	47.85% lignin soluble in ChCl+OA	41
ChC + succinic acid (SA) + glycerol (Gly)	antisolvent	water	reed straw	93.1% glucose yield	46
ChCl + LA, ChCl + EG	antisolvent	water or 50% aqueous acetone	vine shoots	washing with aqueous acetone enhanced delignification by 31.5%	17
ChCL+LA	antisolvent	anhydrous ethanol	sugarcane bagasse		40
ChCl + oxalic acid	antisolvent	anhydrous ethanol	*Triarrhena lutarioriparia*	83.71% glucose yield	47
ChCl + LA ChCL + malonic acid ChCl + glycerol	antisolvent	aqueous ethanol	sugarcane bagasse	81.6% delignification with ChCL+LA	48
ChCl + urea + ethanolamin	solid residue washed with DI water		corncob	55% lignin extracted	49
ChCl + urea		DI water	corn cob	46.09% delignification	38
ChCl + oxalic acid	antisolvent	ethanol	rape straw	96% cellulase digestibility	39
ChCl + LA	antisolvent	anhydrous ethanol	sugarcane bagasse	70.6% biomass component utilization	50
L-cystein + LA	antisolvent	aqueous acetone (50%)	sugarcane bagasse	>80% delignification	4
L-cystein + BSA	hot filtration followed by DI water washing		bamboo	92% delignification	5
ChCl + L-Cys	antisolvent	Aqueous acetone (50%)	tea stem	57.12% lignin recovery; residue containing 53.4% cellulose and 9.16% lignin; EH yield 71.14%.	this work
ChCl + L-Cys	antisolvent	aqueous ethanol (50%)	tea stem	44.91% lignin recovery; residue containing 45.98% cellulose and 14.34% lignin; EH yield 54.29%.	this work
ChCl + L-Cys	antisolvent	water	tea stem	8.54% lignin recovery; residue containing 41.43% cellulose and 19.63% lignin; EH yield 26.83%	this work

coproducts by simultaneously maximizing carbohydrate accessibility and preserving an uncondensed lignin stream.

Dilution with water produced a pronounced change in the recovery-stage solvent environment, accompanied by greater lignin retention within the recovered residue and substantially lower enzymatic accessibility. The spherical deposits and fused surface structures observed by SEM, together with the higher residual lignin content, are consistent with aggregation and redeposition of lignin-rich components onto the recovered residue, thereby restricting substrate accessibility.[28] Aqueous ethanol exhibited an intermediate fractionation behavior, producing localized lignin-rich aggregates together with codeposited carbohydrate-derived components that functioned as competitive adsorption sinks.[19,43] These antisolvent-dependent surface features primarily reflect the physical aggregation and redeposition of lignin-rich components during recovery-stage dilution. In parallel, 2D-HSQC analysis of the recovered lignin fractions revealed distinct variations in lignin interunit architecture, particularly in the β-O-4 and G_2 correlations. These molecular-level variations describe structural differences among the recovered lignin fractions and are considered separately from the physical deposition observed on the pretreated residues. The inhibitory contribution of lignin retained within the solid residues was evaluated independently using R-L_{Ac}, R-L_{EtOH}, and R-L_W. QCM-D analysis revealed pronounced differences in cellulase retention, with R-L_{EtOH} exhibiting up to 81.0% irreversible enzyme adsorption. At the interface, the pronounced cellulase retention despite the negative surface charges of both lignin and enzyme indicates that hydrophobic interactions can outweigh the electrostatic repulsion predicted from the measured zeta potentials. Such persistent nonproductive enzyme retention may increase enzyme demand and consequently reduce overall fractionation efficiency during downstream processing.

Surfactant addition differentiates the two barrier types: T-80 neutralized the localized hydrophobic sinks on the ethanol-treated residue, restoring hydrolysis to ~83%, but did not overcome the steric hindrance caused by water precipitation.[21] This surface inhibition is reflected in an apparent electrostatic inconsistency: although the water and ethanol-derived lignin surfaces were strongly electronegative (−13.9 and −12.25 mV, against −5.78 mV for cellulase), they retained the enzyme most irreversibly (up to 81%). The binding profiles indicate that lignin-associated hydrophobic interactions, potentially reinforced by π−π interactions among exposed aromatic domains, can outweigh the electrostatic repulsion expected between the negatively charged lignin surfaces and cellulase. Consequently, recovery-stage dilution can substantially modify substrate recalcitrance and partially diminish the accessibility generated during the preceding DES pretreatment.[14,36] Antisolvent selection thus constitutes an important recovery-stage process variable for sustainable biomass fractionation: aqueous acetone supports dual-stream biorefining and efficient resource utilization, whereas the tested protic media resulted in lower lignin recovery and reduced accessibility of the cellulosic substrate.

From a process perspective, the downstream recovery of the antisolvent is strongly dependent on its physicochemical properties and the selected process configuration. Water can be recovered and recycled within appropriately integrated biorefinery

https://doi.org/10.1021/acssuschemeng.6c11956
ACS Sustainable Chem. Eng. XXXX, XXX, XXX−XXX

systems; however, its lower volatility (compared to acetone or ethanol) demands a different separation strategy and may impose a greater thermal duty when evaporation-based recovery is employed. Accordingly, although aqueous acetone exhibited favorable fractionation behavior in the present study, its practical advantage should ultimately be evaluated together with solvent recovery efficiency, recyclability, and process energy requirements.

4. CONCLUSIONS

This study demonstrates that post-pretreatment antisolvent dilution is not merely a separation step, but a critical phase-separation event that determines the redistribution of solubilized lignin and associated biomass components during DES fractionation. Under identical pretreatment conditions, aqueous acetone afforded the most favorable fractionation outcome, achieving 57.12% lignin recovery, 53.4% cellulose content, 9.16% residual lignin, and 71.14% enzymatic hydrolysis, whereas water promoted extensive redeposition and reduced enzymatic hydrolysis to 26.83%. The contrasting behaviors arise from antisolvent-dependent phase separation, which governs lignin re-deposition, surface accessibility, steric hindrance, and nonproductive enzyme interactions. Importantly, these findings show that biomass recalcitrance is not determined solely during pretreatment but can be substantially re-established during the subsequent dilution and separation stage. This work therefore identifies recovery-stage phase behavior as an independent design variable, alongside pretreatment severity, for controlling substrate accessibility and lignin quality in DES-based biomass fractionation.

■ ASSOCIATED CONTENT

Supporting Information

The Supporting Information is available free of charge at https://pubs.acs.org/doi/10.1021/acssuschemeng.6c11956.

Experimental details of DES fractionation, lignin recovery, enzymatic hydrolysis, holocellulose extraction, and analytical methods; FTIR spectra of pretreated residues and regenerated lignin; TGA and DTG profiles of untreated and pretreated residues; and 2D NMR structural assignments for lignin linkages and aromatic units (DOCX)

■ AUTHOR INFORMATION

Corresponding Author

Junlong Song − *Jiangsu Co-Innovation Center for Efficient Processing and Utilization of Forest Resources and International Innovation Center for Forest Chemicals and Materials, Nanjing Forestry University, Nanjing 210037, China;* orcid.org/0000-0002-5271-8140; Email: junlong.song@njfu.edu.cn. Tel.:+86-25-85428163. Fax.:+86-25-85428689

Authors

Usama Shakeel − *Jiangsu Co-Innovation Center for Efficient Processing and Utilization of Forest Resources and International Innovation Center for Forest Chemicals and Materials, Nanjing Forestry University, Nanjing 210037, China*

Ying Zeng − *Jiangsu Co-Innovation Center for Efficient Processing and Utilization of Forest Resources and International Innovation Center for Forest Chemicals and Materials, Nanjing Forestry University, Nanjing 210037, China*

Furong Zheng − *Jiangsu Co-Innovation Center for Efficient Processing and Utilization of Forest Resources and International Innovation Center for Forest Chemicals and Materials, Nanjing Forestry University, Nanjing 210037, China*

Jiaqi Guo − *Jiangsu Co-Innovation Center for Efficient Processing and Utilization of Forest Resources and International Innovation Center for Forest Chemicals and Materials, Nanjing Forestry University, Nanjing 210037, China;* orcid.org/0000-0001-7557-0356

Wenyuan Zhu − *Jiangsu Co-Innovation Center for Efficient Processing and Utilization of Forest Resources and International Innovation Center for Forest Chemicals and Materials, Nanjing Forestry University, Nanjing 210037, China*

Mohamed El-Sakhawy − *Cellulose and Paper Department, National Research Centre, Cairo 12622, Egypt;* orcid.org/0000-0002-5095-3112

Carolina Krebs de Souza − *Department of Chemical Engineering, University of Blumenau (FURB), Blumenau, Santa Catarina 89012-900, Brazil*

Complete contact information is available at: https://pubs.acs.org/doi/10.1021/acssuschemeng.6c11956

Notes

The authors declare no competing financial interest.

■ ACKNOWLEDGMENTS

This project was financially supported by the National Natural Science Foundation of China (Grant No. 22478196) and the Priority Academic Program Development of Jiangsu Higher Education Institutions. During the preparation of this work, the author(s) used Google Gemini 2.5 in order to refine the grammar and typos. After using this tool/service, the author(s) reviewed and edited the content as needed and take(s) full responsibility for the content of the published article.

■ REFERENCES

(1) Shakeel, U.; Zeng, Y.; Zheng, F.; Guo, J.; Zhu, W.; Khan, M. R.; El-Sakhawy, M.; de Souza, C. K.; Song, J. From Biomass Deconstruction to Reactive Plasticization: A Trifunctional l-Cysteine Deep Eutectic Solvent for the Closed-Loop Valorization of Tea Stems. *Bioresour. Technol.* **2026**, *455*, No. 134805.

(2) Xu, H.; Peng, J.; Kong, Y.; Liu, Y.; Su, Z.; Li, B.; Song, X.; Liu, S.; Tian, W. Key Process Parameters for Deep Eutectic Solvents Pretreatment of Lignocellulosic Biomass Materials: A Review. *Bioresour. Technol.* **2020**, *310*, No. 123416.

(3) Zhao, Y.; Shakeel, U.; Saif Ur Rehman, M.; Li, H.; Xu, X.; Xu, J. Lignin-Carbohydrate Complexes (LCCs) and Its Role in Biorefinery. *J. Clean. Prod.* **2020**, *253*, No. 120076.

(4) Zhou, X.; Zeng, X.; Hu, S.; Zhou, Y.; Yue, F.; Xie, M. Highly Uncondensed Lignin Extraction in the Novel Green L-Cysteine/Lactic Acid Cosolvent System. *Chem. Eng. J.* **2024**, *497*, No. 154340.

(5) Zhang, F.; Lin, Q.; Lan, W.; Huang, J.; Su, Z.; Yue, F.; Liu, C. Natural Amino Acid-Tailored Deep Eutectic Solvents for Comprehensive Bamboo Valorization under Mild Conditions. *Chem. Eng. J.* **2025**, *525*, No. 170319.

(6) Hu, X.; Sun, Y.; Zhou, J.; Rahman, K. U.; Tang, X.; Chen, Y.; Cui, Z. Green Extraction of Luteolin from Chrysanthemi Indici Flos Using Deep Eutectic Solvents: Mechanistic Insights, Antioxidant Activities, and Synergistic α-Glucosidase Inhibition. *J. Agric. Food Chem.* **2026**, *74* (27), 21311−21320.

(7) Wu, F.; Guan, Q.; Huang, Y.; Li, C. Mechanistic Insights into the Direct Enzymatic Conversion of Oleuropein to Oleacein from Olive Leaves: Natural Deep Eutectic Solvents as a Tunable Reaction Environment. *J. Agric. Food Chem.* **2026**, *74* (29), 23101−23114.
(8) Singh, I. P.; Sharma, A. Natural Deep Eutectic Solvents as Green Extraction Media for Nutritional and Functional Bioactives *J. Agric. Food Chem.* **2026**, *74*, 14758−14793.
(9) Lei, C.; Weng, Q.; Song, P.; Zhu, Y.; Li, L.; Kong, L.; Yan, L. Thiol Modification of β-Glucosidase via N-Methoxycarbonylmaleimide for Enhancement of Catalytic Efficiency and Environmental Tolerance. *J. Agric. Food Chem.* **2026**, *74* (8), 6905−6918.
(10) Zhou, L.; Feng, X.; Li, X.; Kong, X.; Chen, Y.; Zhang, C.; Hua, Y. Endogenous Small Thiol Compounds Induced Disulfide Bond Cleavage and the Improvement of In Vitro Digestibility of Soy Proteins. *J. Agric. Food Chem.* **2026**, *74* (5), 4527−4537.
(11) Lobato-Rodríguez, Á.; Gullón, B.; Romaní, A.; Ferreira-Santos, P.; Garrote, G.; Del-Río, P. G. Recent Advances in Biorefineries Based on Lignin Extraction Using Deep Eutectic Solvents: A Review. *Bioresour. Technol.* **2023**, *388*, No. 129744.
(12) Isci, A.; Kaltschmitt, M. Recovery and Recycling of Deep Eutectic Solvents in Biomass Conversions: A Review. *Biomass Convers. Biorefinery* **2022**, 197−226.
(13) Wang, M.; Fu, X.; Chang, Y.; Wei, J.; Cui, H. Recent Advancements in Deep Eutectic Solvent (DES) Pretreatment: Applications, Mechanisms, and Integration with Emerging Technologies for Biorefinery. *Ind. Crops Prod.* **2025**, *229*, No. 121028.
(14) Zhao, X.; Meng, X.; Ragauskas, A. J.; Lai, C.; Ling, Z.; Huang, C.; Yong, Q. Unlocking the Secret of Lignin-Enzyme Interactions: Recent Advances in Developing State-of-the-Art Analytical Techniques *Biotechnol. Adv.* **2022**, *54*, No. 107830.
(15) Pereira, A.; Hoeger, I. C.; Ferrer, A.; Rencoret, J.; Del Rio, J. C. ; Kruus, K.; Rahikainen, J.; Kellock, M.; Gutiérrez, A.; Rojas, O. J. Lignin Films from Spruce, Eucalyptus, and Wheat Straw Studied with Electroacoustic and Optical Sensors: Effect of Composition and Electrostatic Screening on Enzyme Binding. *Biomacromolecules* **2017**, *18* (4), 1322−1332.
(16) Langley, L. A.; Villanueva, D. E.; Fairbrother, D. H. Quantification of Surface Oxides on Carbonaceous Materials. *Chem. Mater.* **2006**, *18* (1), 169−178.
(17) Cañadas, R.; Duque, A.; Bahíllo, A.; Iglesias, R.; Manzanares, P. Pretreatment of Vine Shoot Biomass by Choline Chloride-Based Deep Eutectic Solvents to Promote Biomass Fractionation and Enhance Sugar Production. *Bioengineering* **2024**, *11* (9), No. 935.
(18) Shakeel, U.; Zhang, Y.; Liang, C.; Wang, W.; Qi, W. Unrevealing the Influence of Reagent Properties on Disruption and Digestibility of Lignocellulosic Biomass during Alkaline Pretreatment. *Int. J. Biol. Macromol.* **2024**, *266*, No. 131193.
(19) Zhao, B. C.; Xu, J. D.; Chen, B. Y.; Cao, X. F.; Yuan, T. Q.; Wang, S. F.; Charlton, A.; Sun, R. C. Selective Precipitation and Characterization of Lignin−Carbohydrate Complexes (LCCs) from Eucalyptus. *Planta* **2018**, *247* (5), 1077−1087.
(20) Shakeel, U.; Zhang, Y.; Topakas, E.; Wang, W.; Liang, C.; Qi, W. Unraveling Interplay between Lignocellulosic Structures Caused by Chemical Pretreatments in Enhancing Enzymatic Hydrolysis. *Carbohydr. Polym.* **2024**, *334*, No. 122037.
(21) Li, R.; Ruan, H.; Zhang, D.; Zhu, C.; Lai, C.; Yong, Q. Tween 80 Reversed Adverse Effects of Combined Autohydrolysis and P-Toluenesulfonic Acid Pretreatment on Enzymatic Hydrolysis of Poplar. *Bioresour. Technol.* **2024**, *393*, No. 130056.
(22) Rahikainen, J. L.; Evans, J. D.; Mikander, S.; Kalliola, A.; Puranen, T.; Tamminen, T.; Marjamaa, K.; Kruus, K. Cellulase-Lignin Interactions-The Role of Carbohydrate-Binding Module and PH in Non-Productive Binding. *Enzyme Microb. Technol.* **2013**, *53* (5), 315−321.
(23) Lai, C.; Yang, B.; Lin, Z.; Jia, Y.; Huang, C.; Li, X.; Song, X.; Yong, Q. New Strategy to Elucidate the Positive Effects of Extractable Lignin on Enzymatic Hydrolysis by Quartz Crystal Microbalance with Dissipation. *Biotechnol. Biofuels* **2019**, *12* (1), 57.
(24) Wang, Y. T.; Zheng, Q. P.; Chai, Y.; Zhang, Y. C.; Zheng, Y. Z. Efficient Pretreatment of Tea Stems Using Biocompatible Ionic Liquid and Monoethanolamine: Toward Improved Enzymatic Hydrolysis and UV-Blocking PVA-LNPs Composite Films. *Chem. Eng. J.* **2025**, *523*, No. 168378.
(25) Cintrón, M. S.; Hinchliffe, D. J. FT-IR Examination of the Development of Secondary Cell Wall in Cotton Fibers. *Fibers* **2015**, *3* (1), 30−40.
(26) Wang, Q.; Tan, X.; Wang, W.; Miao, C.; Sun, Y.; Yuan, Z.; Zhuang, X. KOH/Urea Pretreatment of Bagasse for Ethanol Production without Black Liquor or Wastewater Generation. *Ind. Crops Prod.* **2022**, *178*, No. 114567.
(27) Zahoor; Wang, W.; Tan, X.; Imtiaz, M.; Wang, Q.; Miao, C.; Yuan, Z.; Zhuang, X. Rice Straw Pretreatment with KOH/Urea for Enhancing Sugar Yield and Ethanol Production at Low Temperature. *Ind. Crops Prod.* **2021**, *170*, No. 113776..
(28) Hu, F.; Ragauskas, A. Suppression of Pseudo-Lignin Formation under Dilute Acid Pretreatment Conditions. *RSC Adv.* **2014**, *4* (9), 4317−4323.
(29) De Menezes, F. F.; Rencoret, J.; Nakanishi, S. C.; Nascimento, V. M.; Silva, V. F. N.; Gutiérrez, A.; Del Río, J. C.; De Moraes Rocha, G. J. Alkaline Pretreatment Severity Leads to Different Lignin Applications in Sugar Cane Biorefineries. *ACS Sustainable Chem. Eng.* **2017**, *5* (7), 5702−5712.
(30) Giummarella, N.; Lawoko, M. Structural Basis for the Formation and Regulation of Lignin-Xylan Bonds in Birch. *ACS Sustainable Chem. Eng.* **2016**, *4* (10), 5319−5326.
(31) Lawoko, M.; Henriksson, G.; Gellerstedt, G. Characterization of Lignin-Carbohydrate Complexes from Spruce Sulfite Pulp. *Holzforschung* **2006**, *60* (2), 162−165.
(32) Shakeel, U.; Li, X.; Wang, B.; Geng, F.; Saif, M.; Rehman, U.; Zhang, K.; Xu, J. International Journal of Biological Macromolecules Structural Characterizations of Lignins Extracted under Same Severity Using Different Acids *Int. J. Biol. Macromol.* **2022**, *194*, 204−212.
(33) Ando, D.; Nakatsubo, F.; Takano, T.; Yano, H. Elucidation of LCC Bonding Sites via γ-TTSA Lignin Degradation: Crude Milled Wood Lignin (MWL) from Eucalyptus Globulus for Enrichment of Lignin Xylan Linkages and Their HSQC-NMR Characterization. *Holzforschung* **2016**, *70* (6), 489−494.
(34) Song, Y.; Chandra, R. P.; Zhang, X.; Saddler, J. N. Non-Productive Celluase Binding onto Deep Eutectic Solvent (DES) Extracted Lignin from Willow and Corn Stover with Inhibitory Effects on Enzymatic Hydrolysis of Cellulose. *Carbohydr. Polym.* **2020**, *250*, No. 116956.
(35) Guo, F.; Shi, W.; Sun, W.; Li, X.; Wang, F.; Zhao, J.; Qu, Y. Differences in the Adsorption of Enzymes onto Lignins from Diverse Types of Lignocellulosic Biomass and the Underlying Mechanism. *Biotechnol. Biofuels* **2014**, *7* (1), No. 38.
(36) Huang, C.; Jiang, X.; Shen, X.; Hu, J.; Tang, W.; Wu, X.; Ragauskas, A.; Jameel, H.; Meng, X.; Yong, Q. Lignin-Enzyme Interaction: A Roadblock for Efficient Enzymatic Hydrolysis of Lignocellulosics. *Renewable Sustainable Energy Rev.* **2022**, *154*, No. 111822.
(37) Brandt, A.; Gräsvik, J.; Hallett, J. P.; Welton, T. Deconstruction of Lignocellulosic Biomass with Ionic Liquids. *Green Chem.* **2013**, 550−583.
(38) Yanak, S.; Buyukkileci, A. O. Delignification of Corncob by Choline Chloride-Urea Deep Eutectic Solvent for Enzymatic Production of Xylooligosaccharides. *Ind. Crops Prod.* **2024**, *217*, No. 118894.
(39) Li, X.; Tang, W.; He, Y. C. Integrated Understanding of Acidic Deep Eutectic Solvent Choline Chloride: Oxalic Acid Pretreatment to Enhance the Enzymatic Hydrolysis of Rape Straw. *Ind. Crops Prod.* **2023**, *206*, No. 117691.
(40) Wang, N.; Xu, B.; Wang, X.; Lang, J.; Zhang, H. Chemical and Structural Elucidation of Lignin and Cellulose Isolated Using DES from Bagasse Based on Alkaline and Hydrothermal Pretreatment. *Polymers* **2022**, *14* (14), No. 2756.

https://doi.org/10.1021/acssuschemeng.6c11956
ACS Sustainable Chem. Eng. XXXX, XXX, XXX−XXX

(41) Li, C.; Huang, C.; Zhao, Y.; Zheng, C.; Su, H.; Zhang, L.; Luo, W.; Zhao, H.; Wang, S.; Huang, L. J. Effect of Choline-Based Deep Eutectic Solvent Pretreatment on the Structure of Cellulose and Lignin in Bagasse. *Processes* **2021**, *9* (2), 1−14.
(42) Chen, H.; Jiang, B.; Rahman, M. M.; Shao, T.; Wu, W.; Jin, Y. Direct Determination of the Interaction between Carbohydrate-Binding Modules and Lignin with Different Phenol Hydroxyl Contents. *J. Agric. Food Chem.* **2026**, *74* (27), 21321.
(43) Giummarella, N.; Lawoko, M. Structural Insights on Recalcitrance during Hydrothermal Hemicellulose Extraction from Wood. *ACS Sustainable Chem. Eng.* **2017**, *5* (6), 5156−5165.
(44) Kumar, A. K.; Parikh, B. S.; Pravakar, M. Natural Deep Eutectic Solvent Mediated Pretreatment of Rice Straw: Bioanalytical Characterization of Lignin Extract and Enzymatic Hydrolysis of Pretreated Biomass Residue. *Environ. Sci. Pollut. Res.* **2016**, *23* (10), 9265−9275.
(45) Cui, P.; Ye, Z.; Chai, M.; Yuan, J.; Xiong, Y.; Yang, H.; Yao, L. Effective Fractionation of Lignocellulose Components and Lignin Valorization by Combination of Deep Eutectic Solvent with Ethanol. *Front. Bioeng. Biotechnol.* **2023**, *10*, No. 1115469.
(46) Shao, Y.; Zhang, C.; Wang, J.; Xie, F.; Wang, S.; Yang, R.; Luo, H. Efficient Butanol Bioproduction from Renewable Lignocellulosic Biomass by an Integrated Strategy of Ternary Deep Eutectic Solvent Pretreatment and Clostridial Fermentation: Toward Complete Utilization of Reed Straw. *Front. Microbiol.* **2025**, *16*, No. 1670387.
(47) Yu, Y.; Wang, D.; Chen, L.; Qi, H.; Liu, A.; Deng, M.; Wu, X.; Wang, K. Recyclable Choline Chloride-Based Deep Eutectic Solvent Pretreatment for Accelerated Enzymatic Digestibility of Triarrhena Lutarioriparia. *Ind. Crops Prod.* **2022**, *187*, No. 115542.
(48) Chourasia, V. R.; Pandey, A.; Pant, K. K.; Henry, R. J. Improving Enzymatic Digestibility of Sugarcane Bagasse from Different Varieties of Sugarcane Using Deep Eutectic Solvent Pretreatment. *Bioresour. Technol.* **2021**, *337*, No. 125480.
(49) Xiao, Y.; Qi, J.; Yu, Z.; Zhao, W.; Shao, W.; Li, N.; Kong, Y.; Li, L.; Wei, W. Pretreatment of Corncob Powder by Choline Chloride-Urea-Ethanolamine to Co-Produce Glucose, Xylose and Lignin Nanospheres. *Ind. Crops Prod.* **2023**, *206*, No. 117695.
(50) Gan, P.; Zhang, K.; Xu, Q.; Zhao, Y.; Li, J.; Yang, G.; Zhang, Y.; Wang, Y.; Zhang, L.; Wang, B.; Shang, M.; Chen, J. Microwave-Assisted Choline Chloride/Lactic Acid Pretreatment for High-Efficiency Separation and Value-Added Utilization of Sugarcane Bagasse Components. *Ind. Crops Prod.* **2024**, *220*, No. 119251.

https://doi.org/10.1021/acssuschemeng.6c11956
ACS Sustainable Chem. Eng. XXXX, XXX, XXX−XXX

H208BE49Oan9kkhW_Ercy7Dm3ZL_9Cf3qfKAc485ysgAAALcwgbQGCSqGSIb3DQEHBqCBpjCBowIBADCBnQYJKoZIhvcNAQcBMB4GCWCGSAFlAwQBLjARBAya3EjEE2WkGYusEJkCARCAcLQRRnzDc-RkYC635JbO9o-vbR0nX75g80kp_J6F0Ea4Qlltud8U7oWhRFagFPoZQGzRYMpStU9oewD